UC Irvine
UC Irvine Previously Published Works

Title

Mechanisms that influence the formation of high-ozone regions in the boundary layer downwind of the Asian continent in winter and spring

Permalink

Journal

ISSN

Authors

Kondo, Y
Hudman, RC
Nakamura, K
et al.

Publication Date

DOI

Copyright Information

Peer reviewed

Mechanisms that influence the formation of high-ozone regions in the boundary layer downwind of the Asian continent in winter and spring

Y. Kondo,[1] R. C. Hudman,[2] K. Nakamura,[1,3] M. Koike,[4] G. Chen,[5] Y. Miyazaki,[1] N. Takegawa,[1] D. R. Blake,[6] I. J. Simpson,[6] M. Ko,[5] K. Kita,[7] T. Shirai,[8,9] and S. Kawakami[8]

[1] The seasonal variation of ozone (O_3) in the boundary layer (BL) over the western Pacific is investigated using a chemistry-transport model. The model results for January and April–May 2002 were evaluated by comparison with PEACE aircraft observations. In January, strong northwesterlies efficiently transported NO_x from the continent, leading to an O_3 increase of approximately 5–10 ppbv over a distance of about 3000 km. In April, southwesterlies dominated due to anticyclone development over the western Pacific. Along this flow, O_3 continued to be produced by NO_x emitted from East Asia. This resulted in the formation of a high-O_3 (> 50 ppbv) region extending along the coastal areas of East Asia. This seasonal change in O_3 was driven in part by a change in the net O_3 production rate due to increases in solar UV and H_2O. Its exact response depended on the NO_x values in the BL. The net O_3 production rate increased between winter and spring over the Asian continent and decreased over the remote western Pacific. Model simulations show that about 25% of the total O_3 (of 10–20 ppbv) increase over the coastal region of Northeast Asia was due to local production from NO_x emissions from China, and the rest was due to changes in background levels as well as emissions from Korea, Japan, and east Siberia. Uplift of BL air over Asia, horizontal transport in the free troposphere, and subsidence were the principal mechanisms of transporting Asian O_3 to the central and eastern North Pacific.

1. Introduction

[2] In the troposphere, ozone (O_3) is a principal precursor of the hydroxyl radical (OH), which largely controls the oxidizing capacity of the atmosphere [e.g., *Logan et al.*, 1981; *Thompson*, 1992]. In addition to being a greenhouse gas itself, O_3 indirectly controls, through OH, the lifetime of other trace gases (e.g., methane (CH_4)) that are important to climate change. Surface O_3 also has adverse effects on human health and plants at high concentrations. Ozone is chemically produced in the troposphere by reactions between NO and peroxy radicals generated from oxidation of carbon monoxide (CO), CH_4, and nonmethane volatile organic carbons (NMVOCs) initiated by reaction with OH. NMVOCs play an important role in O_3 formation especially at high NO_x concentrations (NO_x-saturated) [e.g., *Thornton et al.*, 2002; *Kleinman et al.*, 2005]. Nitrogen oxides (NO_x (= NO + NO_2)) are the key catalysts in these cycles.

[3] East Asia is a region where rapidly growing anthropogenic activity is causing dramatic increases in the emissions of these O_3 precursors. Specifically, Asian NO_x emissions are estimated to have increased significantly by a factor of 3 between 1975 and 1998 [*Akimoto*, 2003] and by nearly 40% from 1990 to 2002 [*Streets et al.*, 2003]. NO_x emissions from China are estimated to have made a major contribution to the recent rapid increases in anthropogenic NO_x emissions from East Asia [*Naja and Akimoto*, 2004]. In fact, the NO_2 column observed from the Global Ozone Monitoring Experiment (GOME) revealed that NO_2

[1]Research Center for Advanced Science and Technology, University of Tokyo, Tokyo, Japan.
[2]Division of Engineering and Applied Sciences, Harvard University, Cambridge, Massachusetts, USA.
[3]Now at Faculty of Science and Engineering, Waseda University, Tokyo, Japan.
[4]Department of Earth and Planetary Science, Graduate School of Science, University of Tokyo, Tokyo, Japan.
[5]Langley Research Center, National Aeronautics and Space Administration, Hampton, Virginia, USA.
[6]Department of Chemistry, University of California, Irvine, Irvine, California, USA.
[7]Department of Environmental Science, Graduate School of Science, Ibaraki University, Mito, Ibaraki, Japan.
[8]Earth Observation Research and Application Center, Japan Aerospace Exploration Agency, Tokyo, Japan.
[9]Now at Center for Global Environmental Research, National Institute for Environmental Studies, Ibaraki, Japan.

concentrations increased by $7 \pm 1\%$ a^{-1} from 1996 to 2002 over industrial areas of China [*Irie et al.*, 2005; *Richter et al.*, 2005]. NMVOC emissions from China constitute the dominant fraction of NMVOC emissions in East Asia and are estimated to have increased by about 30% from 1990 to 2000 [*Streets et al.*, 2003]. Emissions of these pollutants from the Asian continent can significantly impact the distribution of O_3 over the western Pacific, downwind of Asia.

[4] Ozone in the BL in Asia increases from winter to spring, similar to other midlatitude locations in the Northern Hemisphere [e.g., *Logan*, 1999; *Davis et al.*, 2003; *Tanimoto et al.*, 2005]. Quantifying the role of O_3 production in its seasonal variation in Asia is therefore important considering the continued increase in precursor emissions in this region.

[5] There have been a series of aircraft campaigns aimed at characterizing the outflow of Asian pollution to the North Pacific, including the NASA Pacific Exploratory Mission (PEM)-West A and B (September–October 1992 and February–March 1994, respectively) [*Hoell et al.*, 1997], the Japan Aerospace Exploration Agency (JAXA) Biomass Burning and Lightning Experiment (BIBLE)-T (April 1998) [*Miyazaki et al.*, 2002], and the NASA Transport and Chemical Evolution over the Pacific (TRACE-P) experiment (February–April 2001) [*Jacob et al.*, 2003]. In addition, the JAXA Pacific Exploration of Asian Continental Emission (PEACE) campaigns [*Kondo et al.*, 2004; *Parrish et al.*, 2004a] were conducted under the framework of the Intercontinental Transport and Chemical Transformation 2002 (ITCT 2K2) project in January and April–May 2002 to examine the seasonal transition of Asian outflow.

[6] Ozone formation ($F(O_3)$) and destruction ($D(O_3)$) rates are interconnected with each other mainly by formation of the hydroperoxy radical (HO_2 radical), which appears in both terms. [e.g., *Klonecki and Levy*, 1997]. The characteristics of this coupled O_3 chemistry in conjunction with transport processes for O_3 precursors have been investigated in a number of analyses and modeling studies based upon the data obtained during the above campaigns [*Crawford et al.*, 1997; *Davis et al.*, 2003; *Kondo et al.*, 2004]. Box model studies, which used measured precursors as input parameters, have identified that net O_3 production ($P(O_3)$) is highest in the BL at extratropical latitudes during winter and spring due to high concentrations of precursors, especially NO_x. However, these analyses have been limited to locations sampled by aircraft campaigns. Here we extend the understanding of coupled O_3 chemistry and the resulting O_3 distributions to the entire western Pacific region using a three-dimensional (3-D) Chemistry and Transport Model (CTM).

[7] CTMs, evaluated with PEM-West-B, TRACE-P, and ozonesonde data, have been used for the analysis of chemical and transport processes over the western Pacific [*Bey et al.*, 2001b; *Liu et al.*, 2002; *Wild et al.*, 2004a]. 3-D CTM calculations have shown a persistent increase in net O_3 production over East Asia [e.g., *Mauzerall et al.*, 2000; *Wild et al.*, 2004a], similar to the box model studies. Over the western Pacific and East Asia, episodic lifting ahead of eastward-moving cold fronts (warm conveyor belts; WCBs) has been identified as the dominant pathway in spring for transporting pollutants from the BL to the free troposphere (FT) [*Bey et al.*, 2001b; *Liu et al.*, 2003; *Miyazaki et al.*, 2003; *Liang et al.*, 2004]. On the other hand, transport in the

BL is mainly controlled by dynamical processes within the BL [*Wild et al.*, 2004a; *Liang et al.*, 2004].

[8] In the present work, we focus on the effects of seasonal variation of mean precursor distributions from winter to late spring on O_3 chemistry in the BL. For this purpose we used GEOS-CHEM [e.g., *Bey et al.*, 2001b] monthly mean values, thereby smoothing out small-scale synoptic disturbances. We first evaluate GEOS-CHEM predictions of O_3 precursor fields using PEACE-A and B aircraft data. The central interest is to understand the dependence of the net O_3 production rate on NO_x, water vapor (H_2O), and solar radiation, which are primary parameters that drive the formation and destruction of O_3. This understanding directly relates to the interpretation of the model-calculated seasonal variation of O_3. We also show the seasonal variation of O_3 transport from Asia across the North Pacific.

2. Observations and the Model Descriptions

[9] Aircraft measurements of O_3 and its precursors, including NO, CO, H_2O, and NMVOCs, were made over the western Pacific in the $20°–45°N$ latitude range in January and April–May 2002 during the PEACE-A and B campaigns, respectively. Thirteen flights were conducted between 6 and 23 January 2002 and 12 flights were conducted between 21 April and 16 May 2002. Details of the PEACE aircraft observations are given in *Kondo et al.* [2004]. In addition to these direct in situ measurements, results from time-dependent photochemical box model calculations [*Kondo et al.*, 2004] were used for comparison with the GEOS-CHEM model. The key reactions for O_3 photochemistry considered in this model are listed in Table 1. In this work, we use concentrations of OH, HO_2, and NO_2 (calculated from NO). We also use $F(O_3)$, $D(O_3)$, and $P(O_3)$ rates calculated by the box model expressed as

$$F(O_3) = (k_4[HO_2] + k_5[CH_3O_2] + k_6[RO_2])[NO] \qquad (1)$$

$$\begin{aligned} D(O_3) = &\left(k_{3a}J(O^1D)[H_2O]/k_{3b}[M] + k_7[OH] + k_8[HO_2]\right)[O_3] \\ &+ (k_{10}[NO][O_3]\{(k_{12}[NO_2][OH]/(k_{11}[NO_2] \\ &+ k_{12}[NO_2][OH])\} \end{aligned} \qquad (2)$$

$$P(O_3) = F(O_3) - D(O_3) \qquad (3)$$

where [ ] denotes the number density of the indicated species, k_i is the reaction rate coefficient for reaction R_i, and M denotes N_2 and O_2. The actinic flux for O_3 photolysis is denoted as $J(O^1D)$. For most of the present analysis, diurnally averaged values of radicals, $F(O_3)$, $D(O_3)$, and $P(O_3)$ were used.

[10] We simulated PEACE observations with the GEOS-CHEM 3-D model of tropospheric chemistry (version 6-01-03; http://www.as.harvard.edu/chemistry/trop/geos/), which was driven by assimilated meteorological observations from the Goddard Earth Observing System (GEOS-3) of NASA's Global Modeling and Assimilation Office (GMAO). This includes a global simulation of $O_3–NO_x–NMHC$ chemistry with a fully coupled $H_2SO_4–HNO_3–NH_3–H_2O$ aerosol

Table 1. Key Reactions in O_3 Photochemistry

(R1)	$O_3 + h\nu \rightarrow O_2 + O(^1D)$
(R2)	$(O(^3P) + O_2 + M \rightarrow O_3 + M$
(R3a)	$O(^1D) + H_2O \rightarrow 2OH$
(R3b)	$O(^1D) + M \rightarrow O(^3P) + M$
(R4)	$HO_2 + NO \rightarrow NO_2 + OH$
(R5)	$CH_3O_2 + NO \rightarrow NO_2 + CH_3O$
(R6)	$RO_2 + NO \rightarrow NO_2 + RO$
(R7)	$O_3 + OH \rightarrow HO_2 + O_2$
(R8)	$O_3 + HO_2 \rightarrow 2O_2 + OH$
(R9)	$HO_2 + HO_2 \rightarrow H_2O_2 + O_2$
(R10)	$NO + O_3 \rightarrow NO_2 + O_2$
(R11)	$NO_2 + h\nu \rightarrow NO + O$
(R12)	$NO_2 + OH + M \rightarrow HNO_3 + M$
(R13)	$N_2O_5 + H_2O(aq) \rightarrow 2HNO_3$

mechanism [*Bey et al.*, 2001a; *Park et al.*, 2004]. Detailed descriptions of the model, as used, are given by *Hudman et al.* [2004]. The uptake coefficient of N_2O_5 ($\gamma_{N_2O_5}$) was specified for different aerosol components and conditions [*Evans and Jacob*, 2005] based on laboratory experiments [*Kane et al.*, 2001; *Hallquist et al.*, 2003; *Thornton et al.*, 2003]. The strong dependence of $\gamma_{N_2O_5}$ on aerosol composition has been observed by aircraft observations over the US [*Brown et al.*, 2006]. A global anthropogenic emission inventory for 1998 was used for the present study. The emission inventories for NO_x, CO, and NMVOCs for the major continents and Asian-subregions are summarized in Table 2. We also compared EDGAR global emissions for 2000 [*Olivier et al.*, 2005] and Asian emissions compiled by *Streets et al.* [2003, 2006] for 2001. Biomass burning emissions were the climatological means described by *Duncan et al.* [2003], with the addition of large fires in Siberia identified from satellite data for April–May 2002 [*Bertschi et al.*, 2004]. The NO_x emissions used for GEOS-CHEM were 14% lower than those of EDGAR, and 16% higher than those of *Streets et al.* for the sub-Asia region. The uncertainty of NO_x emissions from China and East Asia is 23–24% for *Streets et al.* [2003], and the uncertainty of the anthropogenic (fossil and biofuel) NO_x emissions is 50% for EDGAR [*Olivier et al.*, 2001]. GEOS-CHEM was run with a reduced vertical resolution of GEOS-3 meteorological fields (30 σ levels), extending from surface pressure up to 85 hPa (including about 20 layers in the troposphere). For comparison with PEACE aircraft observations, we interpolated model calculations along the flight tracks at the times of the flights. Monthly averaged model calculations with a $2° \times 2.5°$ horizontal resolution were used for the discussion of the photochemistry and transport of O_3 for January and April–May. The GEOS-CHEM model has been used to investigate Asian outflow of O_3 to the northeastern Pacific [*Bey et al.*, 2001b; *Hudman et al.*, 2004; *Liu et al.*, 2002, 2004]. These studies show no obvious bias except for a low spring-time O_3 bias (in the

FT at midlatitudes) of 5–10 parts per billion by volume (ppbv) due to an underestimation of stratospheric input [*Hudman et al.*, 2004].

[11] Fossil fuel and biofuel combustion were the dominant fraction (75%) of the total NO_x emissions. We present results from two principal simulations: the standard simulations as described above and a sensitivity simulation with no anthropogenic (fossil and biofuel combustion) NO_x emissions from China.

3. Meteorological Setting

[12] Brief descriptions of meteorological conditions relevant to the present study are given here. More detailed descriptions of the meteorological conditions are given by *Kondo et al.* [2004] and *Oshima et al.* [2004] for April–May. Figure 1 shows the GEOS-3 monthly mean horizontal winds at 1 and 5 km for January and April 2002. The prominent features in the January 1 km field are the strong northwesterlies over the northern Asian continent and westerlies over the western Pacific, both located north of 30°N. Because of the dominating Siberian high pressure system, wind speeds were higher in January and averaged 8 m s^{-1} around 30°N and 130°E. A small fraction of continental outflow can also be seen bending toward the south, reaching 10°–20°N and in the central Pacific during this period, as is typically seen in winter [*Newell and Evans*, 2000]. For the 20°–30°N region over the Asian continent, the flow is easterly or southerly, transporting maritime air from the central Pacific into this region.

[13] The northwesterlies became rather weak (< 2 m s^{-1}) at 1 km by April, especially in the latitudinal band from 20°–30°N. This is associated with the weakening of the Siberian high and strengthening of the Pacific high pressure system. Around 30°N and 130°E the wind speed was as low as about 2 m s^{-1}. Under these conditions, it takes about 3–5 days for continental air masses to reach 140°E after leaving the coastal region. That is, BL air masses over the western Pacific were more aged in April–May than in January. The continental outflow was southwesterly over the coastal region, transporting pollutants in a northeastward direction. Southerly humid air also flowed into this region and a strong anticyclone was located at ~30°N and 165°E.

[14] During the transition period from winter to springtime Asian monsoons, the frequency of warm air intrusions from the south increased due to the buildup of the Pacific high pressure system. At the same time, vertical mixing became more active due to synoptic-scale disturbances, including uplifted transport (WCBs and convective outflow) associated with frontal systems [*Miyazaki et al.*, 2003; *Oshima et al.*, 2004].

[15] At 5 km, northwesterly or westerly winds dominated between 20°–45°N in January and April. These westerlies rapidly transported O_3 produced over East Asia and across the Pacific Ocean in the FT, as will be discussed in section 7.

4. Mean Concentrations and Model Evaluation of Ozone and Related Species

4.1. Vertical Profiles

[16] To evaluate GEOS-CHEM performance, median values of the GEOS-CHEM calculations of CO, NO_x,

Table 2. Comparison of Anthropogenic NO_x, CO, and NMVOC Emission Estimates (GEOS-CHEM, EDGAR, and Streets)[a,b]

	NO_x, Tg N			CO, Tg CO			NMVOCs, Tg[c]		
	GEOS-CHEM	EDGAR	Streets	GEOS-CHEM	EDGAR	Streets	GEOS-CHEM	EDGAR	Streets
Global	25.7	31	NA	587	533	NA	77.7	137	NA
Europe	5.1	8.2	NA	95	75	NA	11.6	28.7	NA
North America	7.2	6.2	NA	113	87	NA	15.1	23.1	NA
South America	1.4	1.3	NA	40	20	NA	5.69	7.2	NA
Africa	1.2	1.7	NA	44	79	NA	7.36	13.7	NA
Asia	8.3	10.0	7.1	255	232	261	32.2	41.9	18.9
Sub-Asia Region (China, Japan, and Korea)	5.2	6.1	4.5	191	109	164	19.1	19.8	8.6

[a]Anthropogenic emissions are from fossil fuel, biofuel, and industrial processes.

[b]GEOS-CHEM emissions are as described in the text; EDGAR emissions are for 2000 as reported by *Olivier et al.* [2005]; Streets emissions are for 2001 as reported by *Streets et al.* [2003], except CO emissions which were updated to values by *Streets et al.* [2006]. EDGAR and Streets emissions are from $1° \times 1°$ gridded datasets.

[c]GEOS-CHEM and Streets values are the sum of speciated VOC emissions included in the model: ethane, propane, lumped alkanes $\geq C_4$ (molecular weight of butane assumed in this calculation), lumped alkenes $\geq C_3$ (molecular weight of propene assumed in this calculation), acetone, methyl ethyl ketone, formaldehyde, and acetaldehyde. EDGAR emissions are values for total lumped non-methane hydrocarbons (NMHCs).

H_2O, HO_2, $P(O_3)$, and O_3 along the flight tracks were compared with those measured during the PEACE campaigns. The flight tracks are shown by *Parrish et al.* [2004a]. The results of the comparisons are shown in Figure 2 and Table 3 for 30°−45°N in January and April−May. The in situ HO_2 and $P(O_3)$ values were calculated by the photochemical box model based on the observed values as discussed in section 2. Data strongly influenced by local sources (e.g., ship plumes) were excluded from the present analysis.

4.1.1. CO and NO_x

[17] The median CO mixing ratios calculated by GEOS-CHEM agreed with the observations to within
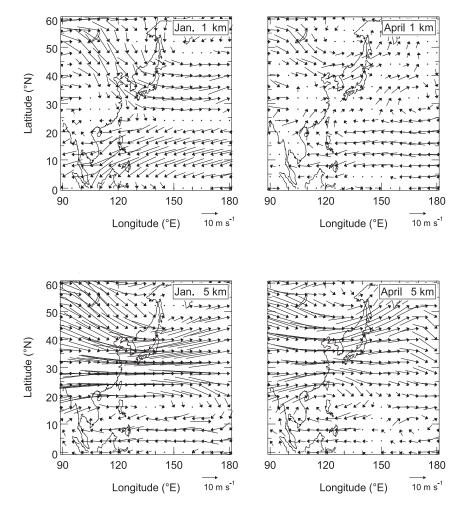

Figure 1. Monthly mean winds input to GEOS-CHEM at 1 and 5 km over East Asia. Values in January are shown on the left and values in April on the right.
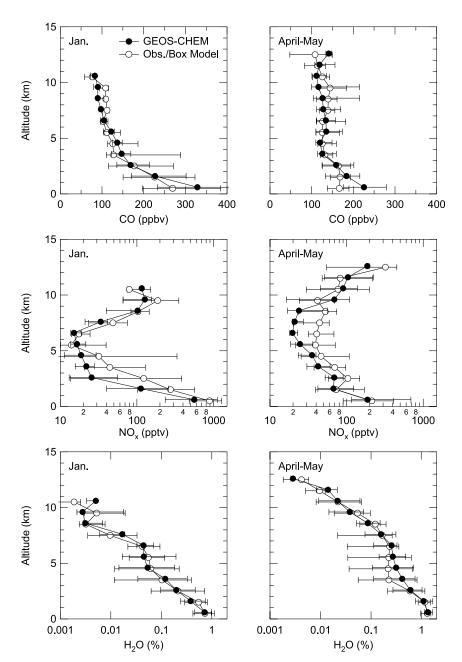
Figure 2. Comparisons of vertical profiles of CO, NO_x, H_2O, HO_2, photochemical O_3 production rates ($P(O_3)$), and O_3 calculated by GEOS-CHEM with those observed or calculated by the photochemical box model during the PEACE campaigns. Solid and open circles represent the GEOS-CHEM-calculated and observed median values, respectively. Horizontal bars represent the central 67th percentile values.

14% at 0–3 km for January and April–May, with a mean bias of about 10%. At the 1-km level, the agreement of the median values degraded to about 20–40%. If we compare the portion of CO that is enhanced above background levels (background values were about 100 ppbv for January and 120 ppbv for April–May), the difference increases to 35% and 230% for January and April–May, respectively. The uncertainty in the present CO emission inventory is estimated to be about 15–25%, based on comparison with other inventories, as shown in Table 2 and in *Ohara et al.* [2007]. In January the observed column-integrated (0–11 km) amounts of CO (2.7×10^{18} molecules cm^{-2}) were very similar to calculations (2.8×10^{18} molecules cm^{-2}). The

relatively high CO mixing ratios in the free troposphere in April–May were mainly caused by active convection over the Asian continent, as identified by PEACE-B observations [*Oshima et al.*, 2004].

[18] The model generally reproduced the observed NO_x for January and April–May. The "C" shaped profile seen in April–May (Figure 2) strongly suggests the influence of convection, lightning, and emissions from commercial aircraft at upper altitudes. The median NO_x mixing ratios calculated by GEOS-CHEM agree with measurements to within about 60% (winter) and 20% (spring) at 1 km. It should also be noted that the largest NO_x variations were observed in the lowest two levels. Overall, GEOS-CHEM
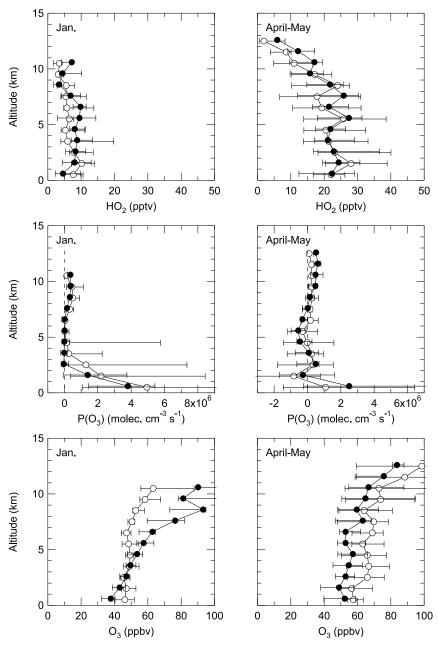
Figure 2. (continued)

underestimated NO_x. Emission of NO_x in East Asia is estimated to have increased by about 20% from 1998 and 2002, while the emission of CO remained unchanged [*Ohara et al.*, 2007]. It is possible that the present calculations, which are based on the 1998 inventory underestimated the NO_x concentrations observed in 2002 by about 20%, although the uncertainty of the emission inventory for each year is comparable.

4.1.2. H_2O and HO_2

[19] H_2O plays a dominant role in O_3 destruction (equation (2)). It is also an initial source of HO_2 as discussed below. GEOS-CHEM reproduced the observed median H_2O mixing ratios to within 1−15% at 0−3 km.

[20] HO_2 is the most important peroxy radical in photochemical O_3 production: previous studies show that over

60% of total photochemical O_3 production is typically from reaction R4 [*Crawford et al.*, 1997; *Kondo et al.*, 2004]. It has been suggested that the heterogeneous loss of HO_2 to aerosol can be an important sink of HO_x [*Jacob*, 2000; *Martin et al.*, 2003a]. The first order rate coefficient k for HO_2 with mean molecular speed ν and gas-phase molecular diffusion coefficient D_g on an aerosol with particle radius R has been estimated as

$$k = \left(R/D_g + 4/\nu\gamma_{HO_2}\right)^{-1}A, \qquad (4)$$

where γ_{HO_2} is the reaction probability of HO_2 [*Martin et al.*, 2003a] and A is the aerosol surface area density. In previous model studies, γ_{HO_2} values ranging between 0.1−0.5 were used [*Dentener et al.*, 1996; *Tie et al.*, 2001; *Liao et al.*,

Table 3. Comparison of GEOS-CHEM Calculations With the In Situ Data[a]

Altitude, km		January				April−May			
		Obs. /Box Model	GEOS-CHEM	Mean Bias	%	Obs. /Box Model	GEOS-CHEM	Mean Bias	%
CO, ppbv	0−3	225	241	18.2	(9.20)	166	189	15.6	(10.3)
	3−6	122	135	5.0	(3.94)	128	127	−4.63	(−3.62)
	6−11	102	93.0	−9.4	(−8.17)	132	122	−8.48	(−6.32)
NO_x, pptv	0−3	429	232	−117	(−49.6)	131	108	−8.31	(−10.4)
	3−6	30.1	19.0	−10.9	(−29.4)	52.0	34.2	−16.9	(−35.3)
	6−11	87.3	78.7	−15.2	(−12.3)	56.7	54.6	−1.75	(−11.2)
HO_2, pptv	0−3	8.59	6.96	−0.60	(−8.51)	24.5	23.2	0.24	(1.06)
	3−6	5.91	8.79	3.10	(48.4)	22.6	23.5	−0.68	(−3.08)
	6−11	4.68	6.32	3.31	(80.8)	16.3	19.0	1.82	(17.6)
$F(O_3)$, 10^6 molec. cm^{-3} s^{-1}	0−3	3.60	2.51	−1.04	(−39.6)	4.33	4.89	0.52	(12.4)
	3−6	0.35	0.36	−0.04	(5.63)	1.54	1.15	−0.37	(−27.1)
	6−11	0.36	0.38	0.02	(46.9)	0.55	0.62	0.01	(10.4)
$D(O_3)$, 10^6 molec. cm^{-3} s^{-1}	0−3	0.68	0.49	−0.10	(−16.6)	4.11	3.65	−0.22	(−7.06)
	3−6	0.18	0.27	0.10	(60.2)	1.51	1.41	−0.22	(−15.0)
	6−11	0.07	0.15	0.07	(122)	0.45	0.40	−0.004	(8.79)
$P(O_3)$, 10^6 molec. cm^{-3} s^{-1}	0−3	2.81	1.72	−0.99	(−60.0)	0.20	0.94	0.72	(−76.8)
	3−6	0.14	−0.005	−0.11	(−104)	−0.03	−0.32	−0.19	(−68.4)
	6−11	0.29	0.24	−0.05	(6.49)	0.23	0.24	0.05	(−24.4)
O_3, ppbv	0−3	46.3	42.6	−4.64	(−10.2)	60.0	51.4	−8.85	(−14.6)
	3−6	49.0	53.5	3.99	(8.65)	65.3	55.0	−9.37	(−14.6)
	6−11	54.4	80.7	25.4	(43.9)	73.0	63.8	−7.08	(−9.71)
H_2O, ppmv	0−3	4987	4320	−430	(−11.7)	10200	10100	337	(5.24)
	3−6	736	726	41.9	(3.92)	2240	3340	170	(8.55)
	6−11	125	145	21.0	(42.4)	1020	956	27.3	(−0.25)

[a]Obs./Box Model and GEOS-CHEM are median values.

2003; *Martin et al.*, 2002a, 2002b, 2003a]. These estimates were based on laboratory experiments made at low temperatures, e.g., 250 K [*Hanson et al.*, 1992; *Cooper and Abbatt*, 1996] or in the presence of Cu^{2+} ions [*Mozurkewich et al.*, 1987]. Heterogeneous loss of HO_2 with $\gamma_{HO_2} = 0.2$ has been estimated to account for 10−40% of total HO_x (= OH + HO_2) radical loss in the boundary layer in polluted regions [*Martin et al.*, 2003a].

[21] On the other hand, based on recent laboratory experiments, the heterogeneous loss of HO_2 to ammonium sulfate is inferred to be strongly temperature dependent [*Thornton and Abbatt*, 2005]. Heterogeneous uptake of HO_2 by aerosol is estimated to be much lower than gas-phase loss of HO_2 at temperatures above 270 K (below about 2 km). These results indicate a need for further laboratory studies on this reaction. For the present GEOS-CHEM model calculations, we neglected heterogeneous loss of HO_2, based on *Thornton and Abbatt* [2005], because we focused on chemical and transport processes in the BL (i.e., < 2 km).

[22] In this context, we compare the predictions from both GEOS-CHEM and the box model. These median model HO_2 values agree to within 6−23% at 0−3 km. There are some large deviations between the GEOS-CHEM photolysis coefficients and those used in the box model, especially when clouds were in the vicinity of the flight tracks. To further assess the modeled HO_2 difference, box model calculations were carried out using actinic flux values and precursor levels predicted from GEOS-CHEM. The results showed less than 5% differences in HO_2 between GEOS-CHEM and the box model, suggesting that there is no fundamental chemical difference between the models. It is noted that recent studies [e.g., *Olson et al.*, 2001, 2004, 2006] have shown that the difference between the HO_2 observations and the box model is typically within 25% for BL conditions.

4.1.3. P(O_3) and O_3

[23] The shapes of the profiles of P(O_3) calculated by GEOS-CHEM generally agree well with those calculated by the box model. P(O_3) is the difference between F(O_3) and D(O_3), each of which is larger than their difference, especially in April−May. The differences between the median values estimated by the box model and GEOS-CHEM (ΔP(O_3)) are 1.2×10^6 and -1.7×10^6 cm^{-3} s^{-1} at 0−1 km in January and April−May, respectively. The respective ΔP(O_3)/F(O_3) ratios are 0.09 and −0.08 in these seasons, indicating that GEOS-CHEM represents O_3 formation and loss well.

[24] In January, GEOS-CHEM largely overestimated O_3 in the upper troposphere. The tropopause height at 30°−45°N in this season was about 11 km [*Kondo et al.*, 2004]. It is possible that the stratosphere-troposphere exchange mechanism may not be well represented by GEOS-CHEM in the region of downwind of the Asian continent for this period. On the other hand in the BL, GEOS-CHEM underestimated O_3 by about 10 ppbv. This discrepancy is generally seen for other surface sites over the western Pacific as will be discussed in section 6.3.

[25] In April−May, GEOS-CHEM underestimated the O_3 values by about 10 ppbv throughout the troposphere. Similar underestimates were found at Trinidad Head, California, USA for April−May during the ITCT 2K2 period, suggesting underestimates of O_3 flux from the stratosphere [*Hudman et al.*, 2004]. By contrast, the GEOS-CHEM CO profile agrees with the observations very well. *Cooper et al.* [2004b] argue that this strong stratospheric O_3 influence in the midtroposphere extends throughout the 38°−43°N latitudinal band, thus similarly affecting PEACE observations at higher latitudes.

4.2. Latitudinal Variation in the BL

[26] Figure 3 compares latitudinal variations of NO_x, H_2O, HO_2, $F(O_3)$, $D(O_3)$, $P(O_3)$, and O_3 values in the BL calculated by GEOS-CHEM, with those observed or calculated by the box model. The comparison was made along the flight track of the PEACE aircraft sampling [*Parrish et al.*, 2004a]. The latitude-longitude range covered by the PEACE observations is shown in Figures 5a and 5b for reference. It should be noted again that the $2° \times 2.5°$ grid resolution of GEOS-CHEM limits the resolution of fine features of the observed plumes, especially for short-lived anthropogenic species like NO_x. GEOS-CHEM nonetheless reproduced the average concentrations and general features of latitudinal and seasonal variations of NO_x. Namely, the model predicted an increase in NO_x with latitude between $22°-36°N$ in January and a general decrease of NO_x from January to April–May north of $30°N$.

[27] GEOS-CHEM reproduced the observed latitudinal variation of the H_2O distribution quite well, especially for January. The increase in H_2O from winter to spring was also reproduced very well. This agreement indicates the reliability of synoptic-scale H_2O fields calculated by the model. The major source of HO_2 is decomposition of H_2O, and a significant HO_2 sink is the HO_2 self reaction (R9), especially over remote Pacific. Therefore good agreement of the HO_2 features is a result of the agreement of measured and modeled H_2O.

[28] The latitudinal variation of $F(O_3)$ as calculated by GEOS-CHEM shows small-scale structures that correspond to those of NO_x. The reproducibility of $F(O_3)$ by GEOS-CHEM depends on that for NO_x. By contrast, the latitudinal variation of $D(O_3)$ is much smoother, especially during winter. The reproducibility of $D(O_3)$ by GEOS-CHEM is better than $F(O_3)$ because GEOS-CHEM reproduces H_2O and HO_2 better than NO_x. Agreement of $P(O_3)$ is somewhat poorer mainly due to the subtraction of large quantities and partly due to the uncertainty in $F(O_3)$, as discussed above. However, GEOS-CHEM predicted latitudinal and seasonal variations of $P(O_3)$ generally well. The GEOS-CHEM O_3 values agree with observed values, mostly to within 10 ppbv, although departures occasionally reach as high as 20 ppbv. These evaluations of horizontal distributions of key species and parameters calculated by GEOS-CHEM provide good estimates for the reliability and limitations of the model results for interpreting O_3 chemistry and transport over the western Pacific.

4.3. Correlations

[29] Comparison of correlations calculated by GEOS-CHEM between key species with those observed gives some further insight in understanding the model performance. Figure 4 compares the calculated NO_x-CO and O_3-CO correlations in the BL with those observed for latitudinal bins of $20°-30°N$ and $30°-45°N$ in January and April–May. In January, the median calculated NO_x-CO correlations agree well (to within $40-100\%$) with those observed except for lowest CO levels (150 ppbv). This suggests that scale of the NO_x plumes at the low CO levels were too small to be represented by GEOS-CHEM. At higher pollution levels (higher CO), the observed median NO_x levels are better reproduced by the model. In April–May, the NO_x levels were much lower than in January and the median

calculated NO_x-CO correlations agree better with those observed at lowest CO levels (150 ppbv), suggesting higher uniformity of NO_x distribution.

[30] Comparison of the observed and calculated O_3-CO correlations show that GEOS-CHEM underestimates O_3 at $30°-45°N$ for most CO ranges both in January and April–May, as anticipated from the discussion made in section 4.1.3. For the January correlation, the data obtained over the Japan Sea during flight 6 made on 13 January are separately shown because the observed O_3 increased by about 15 ppbv with the increase in median CO from 250 to 450 ppbv. The increase in the calculated O_3 was half of that observed. On this day, Siberian high pressure system weakened and the sampled air masses were transported from Northeastern China at $1-1.5$ km (above clouds) without significant changes in altitude. The clear sky conditions at this altitude favored photochemical O_3 formation. During most of the other flights, sampled air masses were transported below 1 km, often below clouds. GEOS-CHEM might not have reproduced the subtle changes in $J(O^1D)$ at smaller scales. This effect will be more significant at lower $J(O^1D)$ conditions at higher latitudes in winter than at lower latitudes and in spring. In fact, the observed increase of O_3 with CO is well reproduced in April–May, despite some bias in the modeled O_3. The calculated O_3-CO correlations at $20°-30°N$ also agree well both in winter and spring, although the number of spring data is limited. Latitudinal and seasonal variation of the O_3 formation rates are discussed in detail in section 5.

5. Photochemistry of Ozone Over East Asia and the Western Pacific

[31] In this section, we analyze the relationship between the spatial and temporal variations of ozone precursors, $F(O_3)$, $D(O_3)$, $P(O_3)$, and O_3 calculated by the GEOS-CHEM model. These variations were driven by variations of precursor transport and chemistry, which were taken into account by the model scheme. Relationships between precursors and $P(O_3)$ over the western Pacific have been investigated in previous studies using box models [*Davis et al.*, 2003; *Crawford et al.*, 1997; *Kondo et al.*, 2004] and 3-D models [*Mauzerall et al.*, 2000; *Pierce et al.*, 2003; *Wild et al.*, 2004a]. In the present study, we show how changes in primary parameters (namely, NO_x, H_2O, and $J(O^1D)$) drive variations in $F(O_3)$ and $D(O_3)$ in the BL over East Asia and the western Pacific. Figures 5a and 5b shows the spatial distributions of key precursors (NO_x, H_2O, and HO_2), $F(O_3)$, $D(O_3)$, and $P(O_3)$ in the BL calculated by GEOS-CHEM. In these figures, the locations where $P(O_3) = 0$ are marked by a thick line for detailed comparison. The flight areas covered by PEACE-A and B observations in the BL are also shown.

5.1. NO_x, H_2O, and HO_2

[32] NO_x mixing ratios in the BL over East Asia are mainly controlled by emissions over East Asian countries (China, Korea, the Japan archipelago, and eastern Siberia), chemical loss ((R12) and (R13)) (hydrolysis of N_2O_5 on aerosols) in Table 1), and transport from source regions, including the effect of dilution. Hydrolysis of N_2O_5 on aerosols is estimated to significantly shorten the NO_x
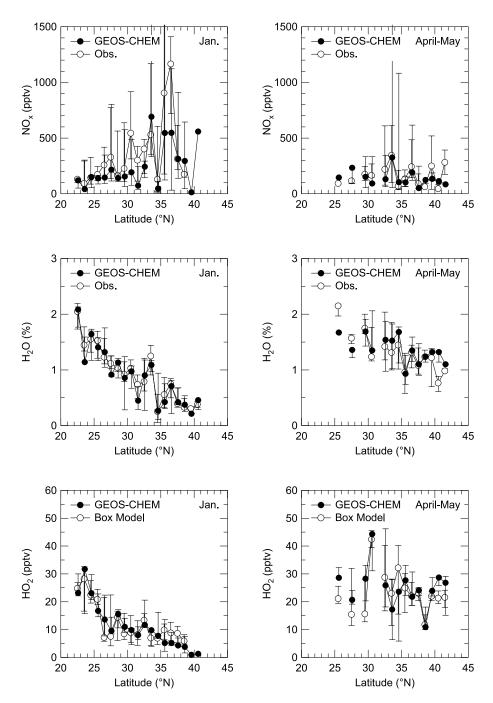
Figure 3. Latitudinal distributions of NO_x, H_2O, HO_2, $F(O_3)$, $D(O_3)$, $P(O_3)$, and O_3 values between 0–2 km in January and April–May. Solid and open circles represent the GEOS-CHEM-calculated median values and those observed or calculated by the box model, respectively.

lifetime in winter, depending on aerosol concentrations [*Tie et al.*, 2001; *Martin et al.*, 2003b; *Takegawa et al.*, 2004].

[33] In January, NO_x concentrations over East Asian sources and the coastal western Pacific at 30°–50°N were much higher than in April due to its longer lifetime, except for eastern Siberia around 50°N, which was affected by biomass burning in April 2002. Moderately high-NO_x (50–100 parts per trillion by volume (pptv)) regions also extended farther over the western Pacific in January due to the stronger north westerlies under lower OH conditions

[*Kondo et al.*, 2004]. The region of moderately high NO_x was significantly reduced in April and the horizontal gradient in NO_x over the western Pacific was steeper in April than in January.

[34] H_2O mixing ratios were generally uniform longitudinally and showed marked latitudinal variations (Figure 5). A region of relatively low H_2O (0.05–1%) west of 150°E shifted northward by about 5° in latitude from January to April due to the combined effects of the increase in temperature and the change in the transport pattern (Figure 1).
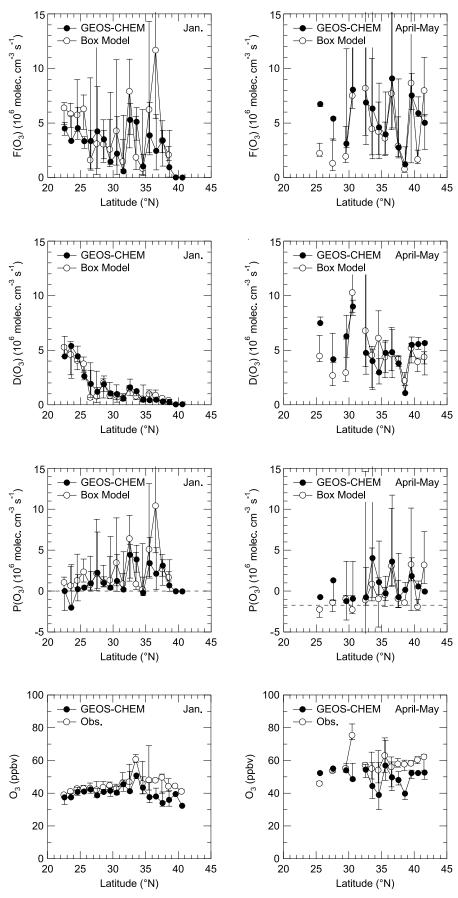
Figure 3. (continued)

[35] The rate of initial formation of $HO_x = OH + HO_2$ ($F(HO_x)$) is expressed as

$$F(HO_x) = 2k_{3a} J(O^1D)[H_2O][O_3]/k_{3b}[M], \qquad (5)$$

indicating that both H_2O and O_3 influence the HO_2 distribution. The HO_2 distribution was more or less uniform longitudinally and had a strong latitudinal gradient, reflecting the H_2O distribution. Some longitudinal variation south of 20°N was caused by the corresponding variation in the O_3 distribution, as discussed in section 6. The latitudinal gradient of HO_2 was driven by changes in H_2O and $J(O^1D)$. The large latitudinal gradient in $J(O^1D)$ at around 30°N was due to changes in the O_3 column associated with a change in the tropopause height [*Crawford et al.*, 1997].

[36] HO_2 also showed a seasonal variation similar to H_2O. The increase in HO_2 from January to April was much more prominent north of 25°N than that at lower latitudes because of the larger increase in $J(O^1D)$ at higher latitudes.

5.2. Production and Loss Rates

[37] $F(O_3)$ and $D(O_3)$ are not independent of each other but are closely coupled, especially through the decomposition of H_2O (R3a), which is the process of O_3 destruction and HO_x formation. The dominant HO_x species are OH and HO_2, with OH playing a key role in $D(O_3)$ while HO_2 contribute to both $D(O_3)$ and $F(O_3)$ (equations (1) and (2)). The effect of this coupling has been discussed by *Klonecki and Levy* [1997] using a box model calculation with CO-CH_4-NO_y-H_2O chemistry. According to their calculations, at NO_x concentrations higher than 300 pptv at the surface at 45°N in July, $P(O_3)$ is positive and increases with increasing H_2O. By contrast, at NO_x concentrations lower than 100 pptv, $P(O_3)$ is negative and further decreases with decreasing H_2O.

[38] We now systematically investigate the seasonal variations of $F(O_3)$, $D(O_3)$, and $P(O_3)$ considering that NO_x, H_2O, and $J(O^1D)$ are the primary driving parameters. In order to extract the effect of changes in $J(O^1D)$ and H_2O on the variations of these quantities, we selected model results in latitudinal bands of 25°–30°N, 30°–35°N, and 35°–40°N because the mixing ratios of H_2O and O_3, and $J(O^1D)$ were rather uniform longitudinally, as discussed above. $F(O_3)$, $D(O_3)$, and $P(O_3)$ are plotted versus NO_x for each latitude band in Figure 6. The $F(O_3)$, $D(O_3)$, and $P(O_3)$ values in each latitudinal band were averaged latitudinally and vertically in the BL for each 2.5° longitudinal spacing between 90°–180°E. We thus obtained 36 data points for each latitudinal band. The curves shown in this figure are smoothed fits to these values. The vertical bars give the central 67% of the difference between the fitted values and the 36 data points, for both low NO_x (< 200 pptv) and high NO_x (> 200 pptv) regimes. The bars are placed at NO_x = 100 pptv and 400 pptv, which are typical NO_x values in each regime. Generally, the slope of the $F(O_3)$-NO_x correlation was proportional to $[HO_2]$ and thus increased from winter to spring. $D(O_3)$ was rather insensitive to NO_x as expected from equation (2). $D(O_3)$ showed an increase

from winter to spring due to the increase in $J(O^1D)$ [H_2O] and resulting HO_2, as discussed above.

[39] Between 25°–30°N at high-NO_x concentrations (> 300 pptv), $P(O_3)$ increased from January to April. Although the rate of the seasonal increase in $F(O_3)$ was higher than that of $D(O_3)$, especially for NO_x level of 300–600 pptv, the slope of the $P(O_3)$-NO_x correlation, and therefore $P(O_3)$, increased because $F(O_3) \gg D(O_3)$. Note that the $P(O_3)$-NO_x correlation is not a linear relation. By contrast $P(O_3)$ decreased from January to April at low NO_x (< 300 pptv). The high-NO_x regime geographically corresponds to the Asian continent and its coastal area and the low-NO_x regime to the remote western Pacific (Figure 5).

[40] Between 30°–35°N and 35°–40°N, in the high-NO_x regime (NO_x > 100–200 pptv), $P(O_3)$ significantly increased from winter to spring, similar to 25°–30°N. In April, the $P(O_3)$-NO_x correlation was similar for all latitudes (25°–40°N) because of the similarity in the $F(O_3)$-NO_x correlation or equivalently HO_2 concentrations. In January, the slope of the $P(O_3)$-NO_x correlation significantly decreased with latitude, mainly due to the latitudinal dependence of the $F(O_3)$-NO_x correlation. This led to the larger seasonal increase in $P(O_3)$ at higher latitudes in the high NO_x regime.

[41] Figure 7 shows the critical NO_x mixing ratio at which $P(O_3) = 0$ (i.e., $(NO_x)_{crit}$) as a function of H_2O and latitude. Generally, H_2O concentration and $J(O^1D)$ decreased with latitude, resulting in a reasonably tight correlation of $(NO_x)_{crit}$ with H_2O. At 20°–25°N, $(NO_x)_{crit}$ increased from about 70 to 120 pptv from January to April. At higher latitude, $(NO_x)_{crit}$ was lower and its seasonal increase was smaller.

[42] The spatial distribution of $P(O_3)$, shown in Figure 5b, can now be interpreted using the derived relationships. Over East Asia and the coastal western Pacific, NO_x was higher than 300 pptv (Figure 5a). In this high-NO_x regime, the spatial and temporal variations of $P(O_3)$ were controlled mainly by variations of $F(O_3)$, because $F(O_3)$ was generally larger than $D(O_3)$ and the magnitude of the variations in $F(O_3)$ were larger than those in $D(O_3)$, as discussed above. For this reason, $P(O_3)$ was persistently positive in winter and spring in this region. The effect of HO_2 in controlling the magnitude of $F(O_3)$ is most clearly seen in the relatively low $F(O_3)$ rates in north-eastern China, Korea, and Japan between 35°–45°N in January despite the high-NO_x values. In April, $F(O_3)$ in this region showed a dramatic increase (up to 20 ppbv day^{-1}) due to the large increase in $J(O^1D)$ [H_2O], despite the decrease in NO_x (Figure 5a). Figure 6 also shows that maximum NO_x decreased by about a factor 2 from January to April.

[43] Over the western Pacific, NO_x was generally lower than 300 pptv. In this low-NO_x regime, the pattern of the $P(O_3)$ distribution showed significant seasonal variations mainly due to the change in the NO_x distribution. A slight increase in $(NO_x)_{crit}$ from winter to spring also played a role. In January, the positive $P(O_3)$ region extended as far as 1000 km downstream of the East Asian countries, to 135°E at 25°N and further to 150°E at 35°N. In April, the region in which $P(O_3) = 0$ over the western Pacific shifted closer to the continent (high-NO_x region) due to the sharper spatial gradient in NO_x at around 100 pptv and an increase in
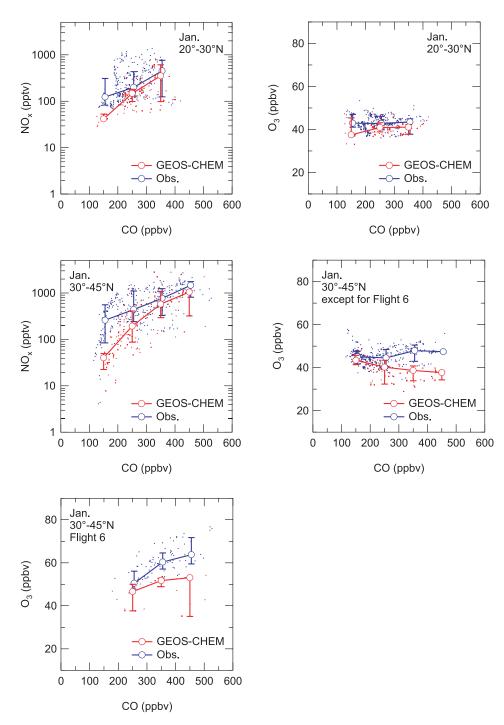
Figure 4. Comparison of the NO_x-CO and O_3-CO correlations in the BL calculated by GEOS-CHEM with those observed at $20°-30°N$ and $30°-45°N$ in (a) January and (b) April–May. The O_3-CO correlations in January are given for flight 6 and for the rest of the flights. The open circles and vertical bars represent the median values and central 67th percentile values, respectively.

$(NO_x)_{crit}$ (Figure 5a). In addition, the gradient in the $P(O_3)$ distribution near the $(NO_x)_{crit}$ region became much sharper in April (Figure 5b).

[44] The southern boundary of the $P(O_3) = 0$ contour overlapped with the southern edge of the relatively low H_2O $(0.05-1.5\%)$ region both in January $(20°-25°N)$ and April $(30°N)$, despite the shift in the boundary's latitude. The NO_x

concentrations in these regions were about $80-120$ pptv (Figure 5a).

6. High-Ozone Regions Over the Western Pacific

6.1. Modeled O_3 Distributions

[45] Here we first interpret the seasonal variation of O_3 distributions by combining O_3, $P(O_3)$, and wind fields. The
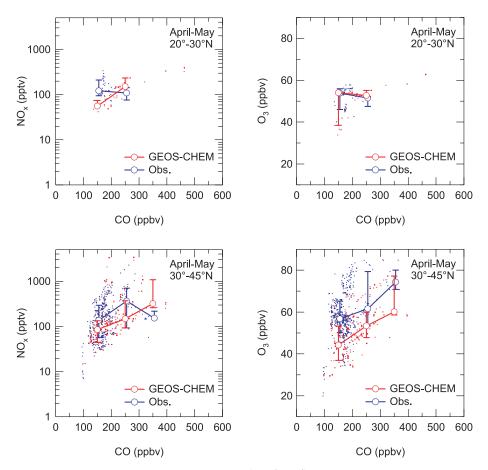
Figure 4. (continued)

calculated O_3 distributions in the BL in January and April are shown in Figure 8, overlaid with the monthly mean wind fields. The boundaries between the net O_3 production and loss regions (i.e., $P(O_3) = 0$) are also shown.

[46] In January, O_3 exceeded 40 ppbv over the western Pacific, forming a high-O_3 region between $20°-35°N$ and $120°-180°E$, downstream of the high-$P(O_3)$ region. North of the high-O_3 region over the Pacific, O_3 levels were $30-35$ ppbv. This is considered to be the extratropical Northern Hemispheric background (NHBG) level, because $P(O_3)$ over Eurasia is close to zero (Figure 5b). Ozone increased above this background by about $5-10$ ppbv during transport over the western Pacific coastal region. The high-O_3 region extended about $2000-3000$ km east of the $P(O_3) = 0$ boundary along the easterly flow.

[47] The anticipated increase in O_3 in winter was estimated by integrating $P(O_3)$ over a distance of about 3000 km along the direction of the average wind field (Figure 8). Dry deposition of O_3 over the surface of the ocean is much smaller than over the continent [e.g., *Hauglustaine et al.*, 1994] and thus neglected. For this calculation, a monthly mean wind speed of about 6 m s^{-1} was assumed. At this speed, an air mass is transported about $2.5°E$ in $0.5-0.8$ days. As shown in Figure 9, the O_3 mixing ratios continued to increase above the NHBG in the $P(O_3) > 0$ region. Ozone predominantly formed west of $135°E$ and then remained constant during further transport to $P(O_3) = 0$ region. During transport in the $P(O_3) > 0$ region, O_3 was

estimated to have increased by about $8-13$ ppbv within $4-6$ days. This estimate is comparable to the total O_3 increase of about 9 ppbv.

[48] The impact of anthropogenic NO_x emissions from different regions of Asia on the O_3 distributions in winter was also estimated from GEOS-CHEM calculations in which anthropogenic NO_x emissions from China were excluded (Figure 8). According to the GEOS-CHEM emission inventory, Japan and Korea together emit NO_x at a rate about half of that of China. For the present analysis, the emissions from China were "turned off" in order to better identify the average transport pathways of NO_x and O_3 by limiting the geographical region. Here we define "China O_3 (C_{O3})" as $C_{O3} = O_3$(full simulation)$-O_3$(no Chinese NO_x). The NO_x emissions from China increased C_{O3} by a few ppbv in the region downwind to $120°-135°E$. The spatial extent of this increase is confined to the region west of $135°E$ due to southward outflow from China, as seen from the monthly mean wind field. Therefore the calculated C_{O3} cannot explain the $5-10$ ppbv increase in O_3 between $135°-180°E$. Air transported to the region east of $135°E$ was impacted more strongly by Japan and Korea, which is reasonable considering the mean flow pattern of air masses transported into this region. NO_x emissions from these countries primarily contribute to the O_3 increase downwind of Asia in the region $135°-180°E$.

[49] In April, a high-O_3 region exceeding 50 ppbv was predicted over the western Pacific (Figure 8). It should be
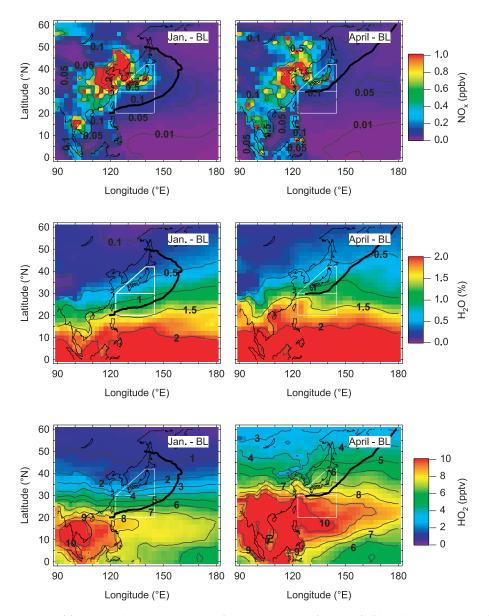
Figure 5. Monthly mean (a) NO_x, H_2O, and HO_2 concentrations and (b) $F(O_3)$, $D(O_3)$, and $P(O_3)$ calculated by GEOS-CHEM between 0–2 km. The locations where $P(O_3) = 0$ are marked by a thick black line. The flight areas covered by PEACE-A and B observations in the BL are shown by white lines.

noted that midlatitude cyclones passed over the western Pacific during the spring portion of the study, as is typical for this season [*Bey et al.*, 2001b; *Miyazaki et al.*, 2003; *Liang et al.*, 2004; *Oshima et al.*, 2004]. The average frequency of midlatitude cyclones was 3–4 per week over the western Pacific during TRACE-P [*Miyazaki et al.*, 2003]. The monthly mean O_3 distributions discussed here includes the effects of vertical and horizontal mixing associated with these synoptic-scale disturbances. The O_3 values were about 40 ppbv in air masses north of 50°N (NHBG-levels), which flowed into the coastal region of East Asia. Ozone is estimated to have increased by about 10 ppbv in the high-O_3 region in comparison with the NHBG. It is difficult to extract typical trajectories for estimating photochemically produced O_3, as was done for January, due to the complexity of the airflows in April

(Figure 8). In addition, dry deposition of O_3 over the Asian continent cannot be neglected [*Hauglustaine et al.*, 1994]. Rather, the effect of O_3 production on the formation of the high-O_3 region is seen from the C_{O3} values. The larger enhancements of O_3 in April than in January due to NO_x emissions from China are expected from the northeastward flows. It is likely that NO_x emissions from Japan and Korea further enhanced the O_3 levels, especially downstream, judging from the different O_3 and C_{O3} distributions. A more quantitative estimate of O_3 formation in East Asia in April is discussed in section 6.2. The boundary between the high- and low-O_3 regions corresponds approximately to the $P(O_3) = 0$ region. Anticyclonic flow with high H_2O confined the high-$P(O_3)$ and high-O_3 region closer to the continent than in January. In addition, the shorter NO_x lifetime also contributed to this shift (Figure 5a). $P(O_3)$
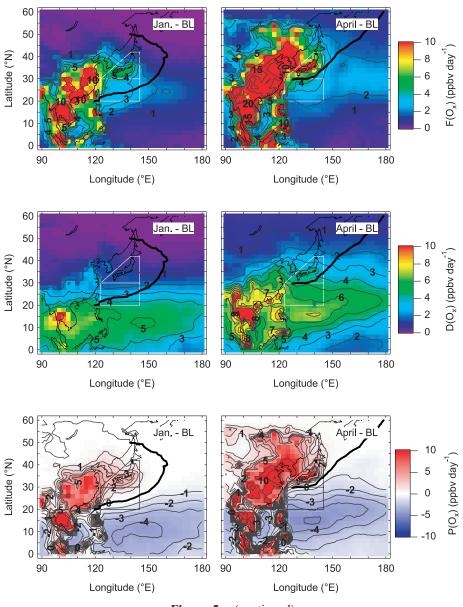
Figure 5. (continued)

increased in the high-NO_x region over the Asian continent (section 5.2), resulting in the highest O_3 levels over the coastal areas of China, Korea, and the Japan archipelago.

[50] It is interesting to note that O_3 levels exceeded 45 ppbv in the region inside the stationary anticyclone centered at 35°N and 170°E. PAN was also calculated to be high in this region (not shown). Trajectory calculations have shown that air masses in the FT over the Asian continent descended in this region. This can be directly seen from the enhancement of C_{O3}. This transport effect is discussed in more detail in section 7.

6.2. Seasonal Variations of Background and East Asian O_3

[51] Previous 3-D CTM studies have often used integrated parameters, e.g., O_3 flux, flux divergence, and average $P(O_3)$ in East Asia for analyses of seasonal O_3 variation in this region [*Mauzerall et al.*, 2000; *Pierce et al.*, 2003;

Wild et al., 2004a]. However, $P(O_3)$ and the resulting O_3 distribution are highly variable horizontally. In this study, instead of using the integrated parameters, we used the monthly mean O_3 distribution in the BL, together with knowledge of the emissions and wind flow to identify factors that control seasonal O_3 variation in Asia and the western Pacific. At extratropical latitudes in the Northern Hemisphere, O_3 concentrations increase from winter to spring due to the increase in net O_3 production [e.g., *Yienger et al.*, 1999; *Hauglustaine et al.*, 2004; *Wild et al.*, 2004b]. We deduced the increase in O_3 due to anthropogenic NO_x emissions in East Asia, except for China, by defining the Non-China O_3 (NC_{O3}) to be the O_3 concentration calculated assuming zero anthropogenic NO_x emissions from China. NC_{O3} includes O_3 formed by reaction of NMVOCs transported from China, although this contribution is not quantified in this study. We now compare three quantities: (1) O_3
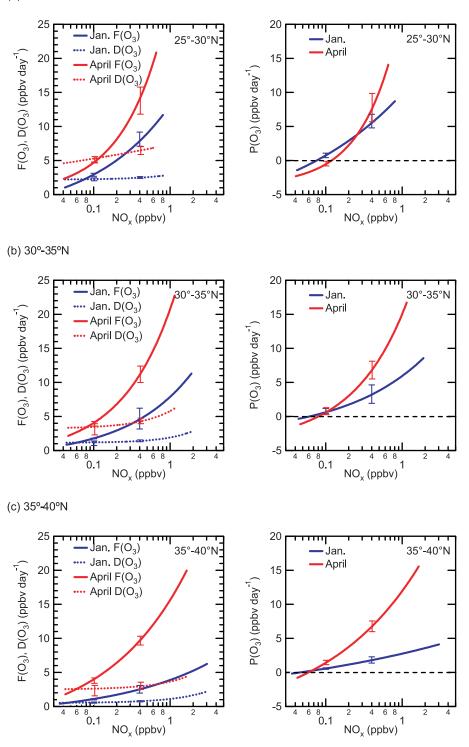
(a) 25°-30°N

(b) 30°-35°N

(c) 35°-40°N

Figure 6. $F(O_3)$, $D(O_3)$, and $P(O_3)$ versus NO_x in the BL for latitudinal bands of $25°-30°N$, $30°-35°N$, and $35°-40°N$ at longitudes of $90°-180°E$ in January and April. The vertical bars represent the central 67th percentile values of the differences between the smoothed fit and individual data points.

change = April O_3−January O_3, (2) NC_{O3} change = April NC_{O3}−January NC_{O3}, and (3) C_{O3} change = April C_{O3}−January C_{O3}. By definition

$$O_3 \text{ change } = [NC_{O3} \text{ change}] + [C_{O3} \text{ change}] \qquad (6)$$

[52] The calculated changes in O_3, NC_{O3}, and C_{O3} are shown in Figures 10a, 10b, and 10c respectively. North of 30°N, the O_3 increase in airflowing from Eurasia into East Asia ($NHBG_{O3}$ change) was about $5-10$ ppbv (Figure 10b). The increase in $NHBG_{O3}$ is consistent with that reported in other 3-D modeling studies that simulated the seasonal
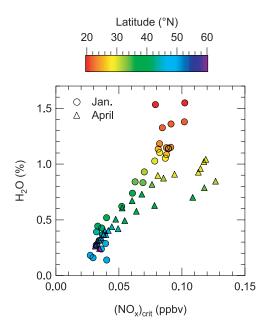
Figure 7. Relationship between $(NO_x)_{crit}$ and H_2O. Latitudes are color coded.

variations of surface O_3 in the Northern Hemisphere [e.g., *Wang et al.*, 1998; *Hauglustaine et al.*, 2004]. By definition [NC_{O3} change]–[$NHBG_{O3}$ change] represents changes in O_3 caused by emissions of precursors in Asia other than China, namely, Japan, Korea, East Siberia, and Southeast Asia. The $NHBG_{O3}$ change contributes about $50 \pm 20\%$ to the total O_3 change ($15-20$ ppbv) over the East China Sea, East Siberia, Korea, and Japan. The fraction of the C_{O3} change to the total O_3 increase is largest over mid and northeastern China (about $50-100\%$), decreasing to about $20-30\%$ over the Sea of Japan. This estimate is independent of the uncertainty in the estimated $NHBG_{O3}$ change. [NC_{O3} change]–[$NHBG_{O3}$ change] was roughly estimated to be about 5 ppbv over the Sea of Japan. This increase is comparable to the change in C_{O3} in this region. In summary, the total O_3 increase of 20 ppbv over the Sea of Japan was caused by about a 10-ppbv increase in $NHBG_{O3}$, a 5-ppbv contribution from China, and a 5-ppbv contribution from the rest of East Asia. Generally, [O_3(full simulation)–O_3(turned off NO_x)] is a low estimate because O_3 production efficiency is higher at lower NO_x levels, leading to artificially high O_3(no NO_x). Therefore it is difficult to rigorously attribute contributions of different countries by this method.

[53] As shown in Figure 8, in January the high-C_{O3} region was located at $10°-30°N$ due to the southward transport of O_3 and its precursors that were produced over China. In April, the high-C_{O3} region shifted to higher latitudes due to the change in the direction of transport, i.e., from southward to northward. The C_{O3} change over the Asian continent was positive north of $25°N$, as seen in Figure 10c, because of the continued increase in C_{O3} from January to April. South of $25°N$, the supply of high C_{O3} from the north, which had prevailed in January, stopped in April, leading to the negative C_{O3} change. In this way, C_{O3} has been demonstrated to be useful in understanding the transport pathways of O_3 originating from China to the surrounding Asian regions.

[54] As described above, we separated the seasonal variation in background O_3 flowing into Asia, O_3 formation from main precursor emitting regions (in this case China), and O_3 formation from the rest of East Asia. This method is advantageous in that we can quantify the combined effect of seasonal variations of transport and chemistry on the BL O_3 concentration. The effect of synoptic-scale disturbances is taken into account by averaging the calculated fields. In the present work we estimated the $NHBG_{O3}$ change to be about 10 ppbv for East Asia, from the O_3 values in the air upstream of East Asia. $NHBG_{O3}$ can be derived more rigorously by turning off precursor emissions for all of East Asia. With an improved estimate of $NHBG_{O3}$, it will be possible to pin-point contributions of each country or specific regions, although the nonlinearity of O_3 formation chemistry as a function of precursor concentrations introduces uncertainties.

6.3. Comparison With the Surface O_3 Data

[55] As discussed in sections 6.1 and 6.2, GEOS-CHEM predicted high-O_3 regions outside the areas of PEACE aircraft observations, especially in January. To evaluate these predictions, we have used long-term surface O_3 measurements made at three sites operated by the Japan Meteorological Agency (JMA) for the Global Atmosphere Watch program of the World Meteorological Organization (WMO/GAW). These sites are Yonagunijima (YON; $24°28'N$, $123°01'E$), Minamitorishima (MNM; $24°17'N$, $153°39'E$), and Ryori (RYO; $39°02'N$, $141°49'E$), as indicated in Figures 8 and 10. They are located over a relatively wide geographical area, where GEOS-CHEM predicts large spatial and temporal variations of O_3 in the BL. It should be noted that the GEOS-CHEM predictions of surface CO have been compared with the CO data obtained at these sites during 2001 [*Liang et al.*, 2004]. The model generally reproduces the observed CO levels, seasonal cycle, and day-to-day variability well, with a negative bias of $5-20$ ppbv in spring.

[56] Figure 11 shows the monthly mean values of O_3 at these sites for 2002. The modeled O_3 values for the BL are also shown for comparison. RYO was predicted to be outside the high-O_3 region in January but within it in April. The GEOS-CHEM model predicted the observed seasonal variation well, providing support for the predicted high-O_3 region in spring.

[57] At MNM, the GEOS-CHEM model predicted the observed seasonal variation of O_3 reasonably well. At YON, GEOS-CHEM significantly underestimated the observed O_3 in January. YON is predicted to be in the region of the steep C_{O3} gradient (Figure 8). The spatial resolution of GEOS-CHEM may not be sufficient to reproduce the fine structures of O_3 distribution in this region.

7. Trans-Pacific Transport of O_3 Produced in Asia

[58] A number of episodes of trans-Pacific long-range transport of CO and O_3 from Asia have been identified over the northeastern Pacific by aircraft and ground-based observations in springtime [*Jaffe et al.*, 2001, 2003a, 2003b; *Jaeglé et al.*, 2003]. *Parrish et al.* [2004b] have reported a long-term increase in springtime background O_3 over the
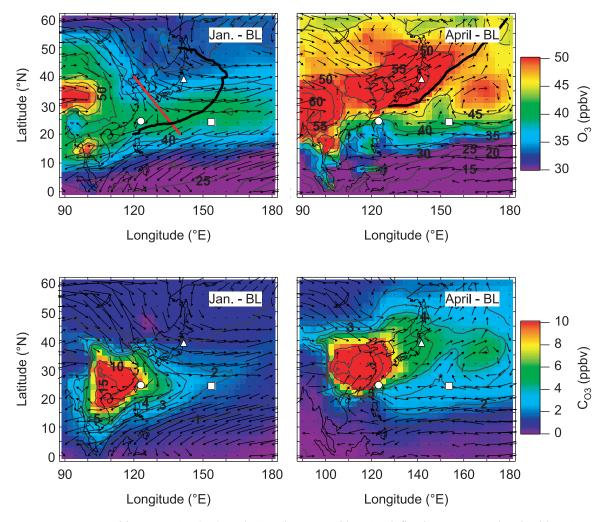
Figure 8. Monthly mean O_3 (top) and C_{O3} (bottom, China-O_3 defined as O_3 associated with NO_x emissions from China) between $0-2$ km overlaid with mean wind fields in January and April. The thick lines in the bottom images represent the locations where $P(O_3)$ is zero. The locations of Yonagunijima, Minamitorishima, and Ryori are marked with a white circle, square, and triangle, respectively. The straight red line for January (top) shows the location along which $P(O_3)$ was integrated.

US west coast during the past 20 years. The impact of Asian anthropogenic pollutant emissions on surface O_3 concentrations in the western United States have been estimated using 3-D CTMs [*Berntsen et al.*, 1994; *Jacob et al.*, 1999]. The principal mechanism of this O_3 transport is subsidence of Asian O_3 transported in the free troposphere. Here we present analysis of O_3 transport from Asia over the entire North Pacific, focusing on its relationship to large-scale meteorological conditions specific to 2002.

[59] Figures 12a, 12b, and 12c show the distributions of C_{O3} at 1.5 and 4.1 km over the Asian continent and the entire North Pacific region for January, April, and May, respectively. Here, $C_{O3} = O_3$(full simulation) $- O_3$(no Chinese NO_x), as defined in section 6. The sea level pressures from National Centers for Environmental Prediction (NCEP) reanalysis data corresponding to these periods are also shown in Figures 13a–13c, for comparison.

[60] Over the East Asian continent and its coastal area, C_{O3} at 1.5 km continued to increase from January to May. The maximum C_{O3} mixing ratio increased from 10 ppbv to 40 ppbv, with the latitude of highest O_3 shifting from 25°N
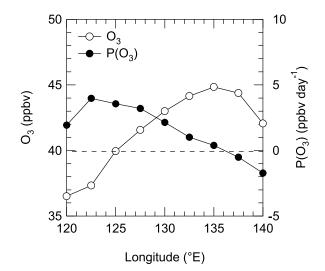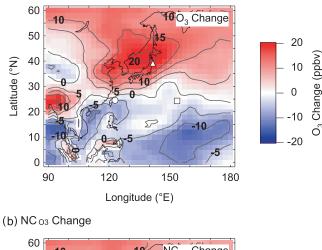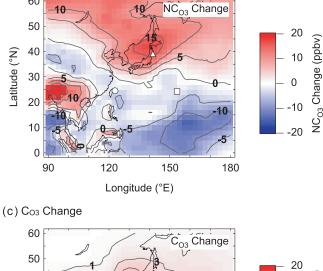

Figure 9. Variations of the monthly mean $P(O_3)$ and O_3 values in the boundary layer along the trajectory shown in Figure 8.
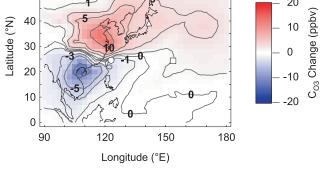
Figure 10. (a) O_3 change = April O_3−January O_3, (b) NC_{O3} change = April NC_{O3}−January NC_{O3}, and (c) C_{O3} change = April C_{O3}−January C_{O3}.

to 30°N during this time. The increase in C_{O3} was due to the increase in $P(O_3)$ in the high-NO_x region, as discussed in section 5.2, as well as direct transport of high O_3 into surrounding regions within the BL. The C_{O3} concentrations at 1.5 km generally decreased with increasing distance from Asia and reached minimum values at around 180°E in January and 200°−210°E in April and May, suggesting that these are the eastern boundaries for the effective transport of

C_{O3} in the BL. East of this boundary C_{O3} started to increase, suggesting another mechanism of transport.

[61] The C_{O3} at 1.5 km showed a broad maximum of 1−2 ppbv in January and 2−3 ppbv in April−May off the west coast of the United States. These C_{O3} values constitute about 2−4% and 3−6% of O_3 in this region in January and April, respectively. A larger scale high pressure system, centered at 220°−230 °E persisted over the eastern Pacific during this study (Figure 13) and has also been observed throughout the year [*Liang et al.*, 2004, Figure 7]. The intensity of the system increased from winter to spring, and in May the system extended over the entire North Pacific region. The region of enhanced C_{O3} clearly corresponds to the region of the high pressure in each season. This high pressure system also prevented BL C_{O3} from being directly transported from Asia further east than 180°−220°E. Even at an altitude of 4.1 km, C_{O3} east of the high pressure system decreased. Transport further east was carried out by flows circulating around the high pressure system from the north. Estimates of O_3 increases over the United States depend on the emission scenarios used. *Jacob et al.* [1999] predicted that a tripling of Asian anthropogenic pollutant emissions from 1985 to 2010 would increase the surface O_3 concentrations by 2−6 ppbv in the western United States. The NO_x emission change used for the present study approximately corresponds to a doubling of the total Asian NO_x emissions from the 1985 level.

[62] In April, C_{O3} was enhanced over the central North Pacific centered at 35°N and 170°E. This enhancement is due to subsidence of free tropospheric air associated with the smaller scale high pressure system centered at the same location (Figure 13b). The horizontal distribution and magnitude of the C_{O3} values at 1.5 and 4.1 km were fairly similar, reflecting subsidence from the free troposphere.

[63] The distribution of C_{O3} at 4.1 km was mainly controlled by frontal uplift of BL air to the free troposphere, followed by eastward advection in spring over the midlatitude western Pacific [e.g., *Bey et al.*, 2001b; *Miyazaki et al.*, 2002; *Cooper et al.*, 2004a; 2004b; *Liang et al.*, 2004]. Indeed, the horizontal distribution of C_{O3} at 4.1 km in April reflects typical transport pathways of WCBs from the southwest to northeast at 120°−150°E. In May, convection also becomes an important mechanism of upward transport, especially over central China [*Oshima et al.*, 2004]. The C_{O3} values at 4.1 km over the entire Pacific generally continued to increase from January to May with the increase in BL C_{O3} values over Asia in conjunction with the increase in convective activities. This resulted in an increase in C_{O3} values at 1.5 km over the west coast of the US through downward transport.

8. Summary and Conclusions

[64] We have improved our understanding of the spatially resolved seasonal variation of O_3 in the BL over the whole Asian continent and western Pacific by combining the monthly mean $P(O_3)$, $P(O_3)$-NO_x correlation, O_3, and C_{O3} (O_3 produced by anthropogenic NO_x emissions from China) calculated by GEOS-CHEM, which was assessed by PEACE observations. Most notably, it was found that, in winter, O_3 formation occurs in a relatively widespread region of the Asian continent and of the western Pacific at
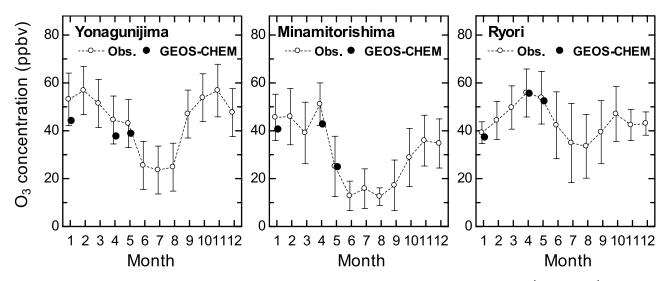
Figure 11. Monthly mean surface O_3 values observed at Yonagunijima (24°28′N, 123°01′E), Minamitorishima (24°17′N, 153°39′E), and Ryori (39°02′N, 141°49′E). Bars represent the 1σ values. The GEOS-CHEM calculated values are also shown for comparison.

midlatitudes due to strong north westerlies, low H_2O, and low $J(O^1D)$. In spring, O_3 formation occurs in a more concentrated region over the Asian continent and its vicinity, with much higher production rates due to higher H_2O and $J(O^1D)$. This seasonal variation of $P(O_3)$ has been shown to cause a seasonal shift in the locations of high O_3 region over the western Pacific. Changes in Northern

Hemispheric background O_3 (NHBG$_{O3}$), C_{O3}, and Non-China O_3 (NC$_{O3}$) made comparable contributions to the springtime O_3 increase over the coastal region of Northeast Asia. Using C_{O3} as a tracer, we have also identified that the downward transport of O_3 from the free troposphere is an effective pathway for long-range transport of the Asian O_3
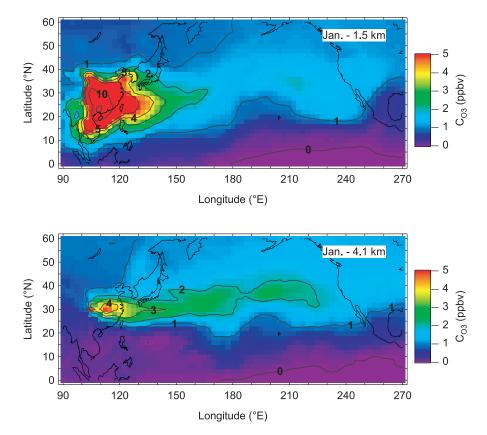

Figure 12. Monthly mean O_3 values at 1.5 km and 4.1 km formed by NO_x emitted from China (C_{O3}) for (a) January, (b) April, and (c) May.

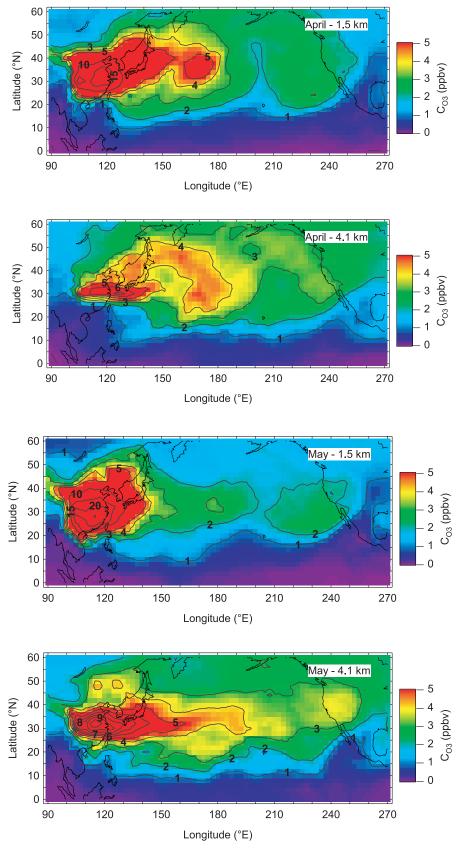KONDO ET AL.: WESTERN PACIFIC HIGH OZONE
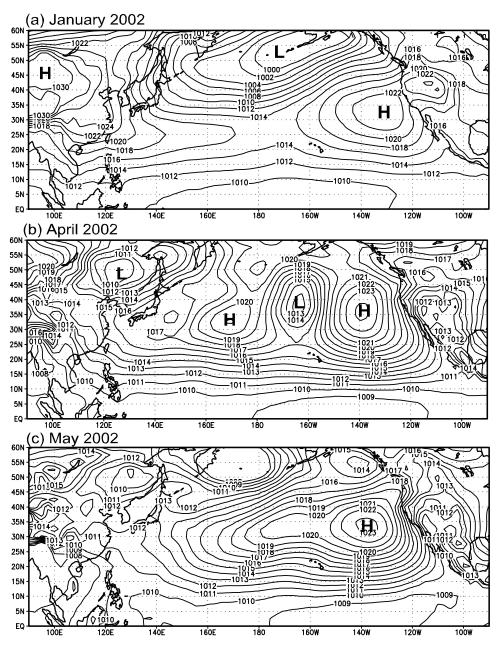

Figure 12. (continued)

Figure 13. Monthly mean sea level pressure over the North Pacific in (a) January, (b) April, and (c) May 2002.

to the mid and central Pacific. The discussion supporting these conclusions is summarized below.

[65] GEOS-CHEM results over the western Pacific for January and April–May 2002 were evaluated using PEACE aircraft data and box model results obtained for the same periods. The median concentrations of O_3 and its precursors calculated by GEOS-CHEM generally agreed well with the observed values (for example, 20–40% for CO, 20–60% for NO_x, and 4–90% for HO_2 at 1 km). The latitudinal and seasonal variations of NO_x, H_2O, HO_2, $F(O_3)$, $D(O_3)$, $P(O_3)$, and O_3 values in the BL (0–2 km) calculated by GEOS-CHEM generally reproduced observed values or those calculated by the box model, providing good estimates of the reliability and limitations of the discussion of O_3 chemistry and transport over the western Pacific.

[66] In the BL, $F(O_3)$ and $D(O_3)$ were closely coupled through the decomposition of H_2O, which destroys O_3 and forms HO_x. The dependence of $F(O_3)$ and $D(O_3)$ on primary driving parameters (NO_x, H_2O, and $J(O^1D)$) was derived by selecting data sets with nearly constant O_3 and $J(O^1D)$ [H_2O] values at different latitudinal bands over Asia and the western Pacific. The slope of the $F(O_3)$-NO_x correlation, which is proportional to [HO_2], increased from winter to spring. In the high-NO_x regime (NO_x > 100–300 pptv, depending on latitudes), the slope of the $P(O_3)$-NO_x, and therefore, $P(O_3)$ increased because $F(O_3) \gg D(O_3)$. By contrast $P(O_3)$ decreased at lower NO_x concentrations. The seasonal variation of $P(O_3)$ in different regions can be understood systematically by this relationship.

[67] GEOS-CHEM predicted that in January, a high-O_3 (~40 ppbv) belt formed between $20°-35°N$, south of the Japan archipelago, and extended to about 5000 km east of the Asian continent. About $5-10$ ppbv of O_3 was produced due to the efficient transport of NO_x by strong northwest-erlies over a distance of about 3000 km within $3-4$ days. NO_x emissions from China mainly contribute to O_3 formation between $120°$ and $135°E$, while emissions from Japan and Korea contributed to the O_3 formation between $135°$ and $180°E$.

[68] In April, southwesterly winds dominated due to the development of an anticyclone over the western Pacific. These flows transported NO_x and O_3 northeastward from northeastern China. Ozone continued to be produced by NO_x emitted from Japan and Korea during transport over distances of about 3000 km, leading to enhanced O_3 (> 50 ppbv) in the regions of China, Korea, and the Japan archipelago. Southwesterly flows, which contained low O_3 levels that were associated with the stationary anticyclone, formed the eastern boundary of the high-O_3 and $P(O_3)$ regions.

[69] This seasonal variation of O_3 was decomposed into seasonal variations of C_{O3} and NC_{O3} by taking the difference of the GEOS-CHEM results between January and April. The NC_{O3} change was the sum of $NHBG_{O3}$ change and changes in O_3 caused by emissions of precursors in East Asian countries other than China. An estimated 25% of the total O_3 increase over the coastal region of Northeast Asia (of $15-20$ ppbv) was caused by the increase in C_{O3}; 50% due to changes in $NHBG_{O3}$; and the rest due to emissions from Korea, Japan, and east Siberia.

[70] In January, the high-C_{O3} region was located at $10°-30°N$ due to southward transport of O_3 and its precursors produced over China. In April, the high-C_{O3} region shifted to higher latitudes due to northward transport. The seasonal variation of the transport pattern is clearly reflected in the distribution of the C_{O3} change over the Asian continent. This method is advantageous for quantifying the combined effect of seasonal variations of transport and chemistry on the BL O_3 concentration.

[71] The levels of O_3 produced by anthropogenic emissions from China increased over the East Asian continent from January to May due to the increase in $P(O_3)$ with increasing $J(O^1D)$ and H_2O. The produced O_3 was transported to the free troposphere mainly by WCBs, followed by rapid advection across the Pacific Ocean by strong westerlies. Subsidence of the advected O_3 in the large-scale high pressure system over the eastern Pacific led to a C_{O3} increase of about 2 ppbv at 1.5 km in spring over the US west coast. In April, the high pressure system located over the central Pacific caused a much larger increase of C_{O3} at 1.5 km due to the higher free tropospheric C_{O3} concentrations. Uplift of BL air over Asia, horizontal transport, and subsidence were shown to be the principal mechanisms of transporting Asian O_3 to the central and eastern North Pacific.

References

Akimoto, H. (2003), Global air quality and pollution, *Science*, *302*, 1716–1719.

Berntsen, T. K., S. Karlsdóttir, and D. A. Jaffe (1994), Influence of Asian emissions on the composition of air reaching the North Western United States, *Geophys. Res. Lett.*, *26*, 2171–2174.

Bertschi, I. T., D. A. Jaffe, L. Jaeglé, H. U. Price, and J. B. Dennison (2004), PHOBEA/ITCT 2002 airborne observations of transpacific transport of ozone, CO, volatile organic compounds, and aerosols to the northeast Pacific: Impacts of Asian anthropogenic and Siberian boreal fire emissions, *J. Geophys. Res.*, *109*, D23S12, doi:10.1029/2003JD004328.

Bey, I., D. J. Jacob, R. M. Yantosca, J. A. Logan, B. D. Field, A. M. Fiore, Q. Li, H. Y. Liu, L. J. Mickley, and M. G. Schultz (2001a), Global modeling of tropospheric chemistry with assimilated meteorology: Model description and evaluation, *J. Geophys. Res.*, *106*, 23,073–23,097.

Bey, I., D. J. Jacob, J. A. Logan, and R. M. Yantosca (2001b), Asian chemical outflow to the Pacific: Origins, pathways and budgets, *J. Geophys. Res.*, *106*, 23,097–23,114.

Brown, S. S., et al. (2006), Variability in nocturnal nitrogen oxide processing and its role in regional air quality, *Science*, *311*, 67–70.

Cooper, P. L., and J. P. D. Abbatt (1996), Heterogeneous interactions of OH and HO_2 radicals with surfaces characteristic of atmospheric particulate matter, *J. Phys. Chem.*, *100*, 2249–2254.

Cooper, O. R., et al. (2004a), A case study of transpacific warm conveyor belt transport: Influence of merging airstreams on trace gas import to North America, *J. Geophys. Res.*, *109*, D23S08, doi:10.1029/2003JD003624.

Cooper, O., et al. (2004b), On the life cycle of a stratospheric intrusion and its dispersion into polluted warm conveyor belts, *J. Geophys. Res.*, *109*, D23S09, doi:10.1029/2003JD004006.

Crawford, J. H., et al. (1997), An assessment of ozone photochemistry in the extratropical western North Pacific: Impact of continental outflow during the late winter/early spring, *J. Geophys. Res.*, *102*, 28,469–28,487.

Davis, D. D., et al. (2003), An assessment of western North Pacific ozone photochemistry based on springtime observations from NASA's PEM-West B (1994) and TRACE-P (2001) field studies, *J. Geophys. Res.*, *108*(D21), 8829, doi:10.1029/2002JD003232.

Dentener, F. J., G. R. Carmichael, Y. Zhang, J. Lelieveld, and P. J. Crutzen (1996), Role of mineral aerosol as a reactive surface in the global troposphere, *J. Geophys. Res.*, *110*, 22,869–22,889.

Duncan, B. N., R. V. Martin, A. C. Staudt, R. Yevich, and J. A. Logan (2003), Interannual and seasonal variability of biomass burning emissions constrained by satellite observations, *J. Geophys. Res.*, *108*(D2), 4100, doi:10.1029/2002JD002378.

Evans, M. J., and D. J. Jacob (2005), Impact of new laboratory studies of N_2O_5 hydrolysis on global model budgets of tropospheric nitrogen oxides, ozone, and OH, *Geophys. Res. Lett.*, *32*, L09813, doi:10.1029/2005GL022469.

Hallquist, M., D. J. Stewart, S. K. Stewart, S. K. Stephenson, and R. A. Cox (2003), Hydrolysis of N_2O_5 on sub-micron sulfate aerosol, *Phys. Chem. Chem. Phys.*, *5*, 3453–3463.

Hanson, D. R., J. B. Burkholder, C. J. Howard, and A. R. Ravishankara (1992), Measurement of OH and HO_2 radical uptake coefficients on water and sulfuric acid surfaces, *J. Phys. Chem.*, *96*, 4979–4985.

Hauglustaine, D. A., C. Granier, G. P. Brasseur, and G. Megie (1994), The importance of atmospheric chemistry in the calculation of radiative forcing on the climate system, *J. Geophys. Res.*, *99*, 1173–1186.

Hauglustaine, D. A., F. Hourdin, L. Jourdaine, M.-A. Filiberti, S. Walters, J.-F. Lamarque, and E. A. Holland (2004), Interactive chemistry in the Labotatoire de Météologie Dynamique general circulation model: Description and background tropospheric chemistry evaluation, *J. Geophys. Res.*, *109*, D04314, doi:10.1029/2003JD003957.

Hoell, J. M., D. D. Davis, S. C. Liu, R. E. Newell, H. Akimoto, R. J. McNeal, and R. J. Bendula (1997), The Pacific Exploratory Mission-West Phase B: February–March, 1994, *J. Geophys. Res.*, *102*, 28,223–28,239.

Hudman, R. C., et al. (2004), Ozone production in transpacific Asian pollution plumes and implications for ozone air quality in California, *J. Geophys. Res.*, *109*, D23S10, doi:10.1029/2004JD004974.

Irie, H., et al. (2005), Evaluation of long-term tropospheric NO_2 data obtained by GOME over East Asia in 1996–2002, *Geophys. Res. Lett.*, *32*, L11810, doi:10.1029/2005GL022770.

Jacob, D. (2000), Heterogeneous chemistry and tropospheric ozone, *Atmos. Environ.*, *34*, 2131–2159.

Jacob, D. J., J. A. Logan, and P. P. Murti (1999), Effect of rising Asian emissions on surface ozone in the United States, *Geophys. Res. Lett.*, *26*, 2175–2178.

Jacob, D. J., et al. (2003), Transport and chemical evolution over the Pacific (TRACE-P) aircraft mission: Design, execution, and first results, *J. Geophys. Res.*, *108*(D20), 9000, doi:10.1029/2002JD003276.

Jaeglé, L., D. A. Jaffe, H. U. Price, P. Weiss-Penzias, P. I. Palmer, M. J. Evans, D. J. Jacob, and I. Bey (2003), Sources and budgets for CO and O_3 in the Northeast Pacific during the spring of 2001: Results from the PHOBEA-II Experiment, *J. Geophys. Res.*, *108*(D20), 8802, doi:10.1029/2002JD003121.

Jaffe, D., T. Anderson, D. Covert, B. Trost, J. Danielson, W. Simpson, D. Blake, J. Harris, and D. Streets (2001), Observations of ozone and related species in the northeast Pacific during the PHOBEA campaigns 1. Ground-based observations at Cheeka Peak, *J. Geophys. Res.*, *106*, 7449–7461.

Jaffe, D., I. McKendry, T. Anderson, and H. Price (2003a), Six "new" episodes of trans-Pacific transport of air pollutants, *Atmos. Environ.*, *37*, 391–404.

Jaffe, D., H. Price, D. D. Parrish, A. Goldstein, and J. Harris (2003b), Increasing background ozone during spring on the west coast of North America, *Geophys. Res. Lett.*, *30*(12), 1613, doi:10.1029/2003GL017024.

Kane, S. M., F. Caloz, and M. T. Leu (2001), Heterogeneous uptake of gaseous N_2O_5 by $(NH_4)_2SO_4$, NH_4HSO_4 and H_2SO_4 aerosol, *J. Phys. Chem.*, *105*, 6465–6470.

Kleinman, L. I., P. H. Daum, Y.-N. Lee, L. J. Nunnermacker, S. R. Springston, J. W. Weinstein-Lloyd, and J. Rudolph (2005), A comparative study of ozone production in five U.S. metropolitan areas, *J. Geophys. Res.*, *110*, D02301, doi:10.1029/2004JD005096.

Klonecki, A., and H. Levy II (1997), Tropospheric chemical ozone tendencies in CO-CH_4-NO_y-H_2O system: Their sensitivity to variations in environmental parameters and their application to a global chemistry and transport model study, *J. Geophys. Res.*, *102*, 21,221–21,237.

Kondo, Y., et al. (2004), Photochemistry of ozone over the western Pacific from winter to spring, *J. Geophys. Res.*, *109*, D23S02, doi:10.1029/2004JD004871.

Liang, Q., L. Jaeglé, D. A. Jaffe, P. Weiss-Penzias, and A. Heckman (2004), Long-range transport of Asian pollution to the northeast Pacific: Seasonal variations and transport pathways of carbon monoxide, *J. Geophys. Res.*, *109*, D23S07, doi:10.1029/2003JD004402.

Liao, H., P. J. Adams, J. H. Seinfeld, L. J. Mickley, and D. Jacob (2003), Interactions between tropospheric chemistry and aerosols in a unified GCM simulation (2003), *J. Geophys. Res.*, *108*(D1), 4001, doi:10.1029/2001JD001260.

Liu, H., D. J. Jacob, L. Y. Chan, S. J. Oltmans, I. Bey, R. M. Yantosca, J. M. Harris, B. N. Duncan, and R. V. Martin (2002), Sources of tropospheric ozone along the Asian Pacific Rim: An analysis of ozonesonde observations, *J. Geophys. Res.*, *107*(D21), 4573, doi:10.1029/2001JD002005.

Liu, H., D. J. Jacob, I. Bey, R. M. Yantosca, B. N. Duncan, and G. W. Sachse (2003), Transport pathways for Asian pollution outflow over the Pacific: Interannual and seasonal variations, *J. Geophys. Res.*, *108*(D20), 8786, doi:10.1029/2002JD003012.

Liu, H., D. J. Jacob, J. E. Dibb, A. M. Fiore, and R. M. Yantosca (2004), Constraints on the sources of tropospheric ozone from ^{210}Pb-^7Be-O_3 correlations, *J. Geophys. Res.*, *109*, D07306, doi:10.1029/2003JD003988.

Logan, J. A. (1999), An analysis of ozonesonde data for the troposphere: Recommendations for testing 3-D models and development of a gridded climatology for tropospheric ozone, *J. Geophys. Res.*, *104*, 16,115–16,149.

Logan, J. A., M. J. Prather, S. C. Wofsy, and M. B. McElroy (1981), Tropospheric Chemistry: A global perspective, *J. Geophys. Res.*, *86*, 7210–7254.

Martin, R. V., et al. (2002a), An improved retrieval of tropospheric nitrogen oxide from GOME, *J. Geophys. Res.*, *107*(20), 4437, doi:10.1029/2001JD001027.

Martin, R. V., et al. (2002b), Interpretation of TOMS observations of tropical tropospheric ozone with a global model and in situ observations, *J. Geophys. Res.*, *107*(D18), 4351, doi:10.1029/2001JD001480.

Martin, R. V., D. J. Jacob, and R. M. Yantosca (2003a), Global and regional decreases in tropospheric oxidants from photochemical effects of aerosols, *J. Geophys. Res.*, *108*(D3), 4097, doi:10.1029/2002JD002622.

Martin, R. V., D. J. Jacob, K. Chance, T. P. Kurosu, P. I. Palmer, and M. J. Evans (2003b), Global inventory of nitrogen oxide emissions constrained by space-based observations of NO_2 columns, *J. Geophys. Res.*, *108*(D17), 4357, doi:10.1029/2003JD003453.

Mauzerall, D. L., D. Narita, H. Akimoto, L. Horowitz, S. Walters, D. A. Hauglustaine, and G. Brasseur (2000), Seasonal characteristics of tropospheric ozone production and mixing ratios over East Asia: A global three-dimensional chemical transport model analysis, *J. Geophys. Res.*, *105*(D14), 17,895–17,910.

Miyazaki, Y., K. Kita, Y. Kondo, M. Koike, M. Ko, W. Hu, S. Kawakami, D. R. Blake, and T. Ogawa (2002), Springtime photochemical ozone production observed in the upper troposphere over East Asia, *J. Geophys. Res.*, *107*(D3), 8398, doi:10.1029/2001JD000811.

Miyazaki, Y., et al. (2003), Synoptic-scale transport of reactive nitrogen over the western Pacific in spring, *J. Geophys. Res.*, *108*(D20), 8788, doi:10.1029/2002JD003248.

Mozurkewich, M., P. H. McMurry, A. Gupta, and J. G. Calvert (1987), Mass accommodation coefficient for HO_2 radicals on aqueous particles, *J. Geophys. Res.*, *92*, 4163–4170.

Naja, M., and H. Akimoto (2004), Contribution of regional pollution and long-range transport to the Asia–Pacific region: Analysis of long-term ozonesonde data over Japan, *J. Geophys. Res.*, *109*, D21306, doi:10.1029/2004JD004687.

Newell, R. E., and M. J. Evans (2000), Seasonal changes in pollutant transport to the North Pacific: The relative importance of Asian and European sources, *Geophys. Res. Lett.*, *27*(16), 2509–2512, doi:10.1029/2000GL011501.

Ohara, T., H. Akimoto, J. Kurokawa, N. Horii, K. Yamaji, X. Yan, and T. Hayasaka (2007), An Asian emission inventory of anthropogenic emission sources for the period 1980–2020, *Atmos. Chem. Phys.*, *7*, 4419–4444.

Olivier, J. G. J., J. J. M. Berdowski, J. A. H. W. Peters, J. Bakker, A. J. H. Visschedijk, and J. P. J. Bloos (2001), Applications of EDGAR. Including a description of EDGAR 3.2: Reference database with trend data for 1970-1995, Natl. Inst. of Public Health and the Environ. (RIVM), RIVM Rep. 773301 001, Bilthoven, Netherlands. (Available at www.rivm.nl/bibliotheek/rapporten/410200051.html)

Olivier, J. G. J., J. A. Van Aardenne, F. Dentener, L. Ganzeveld, and J. A. H. W. Peters (2005), Recent trends in global greenhouse gas emissions: Regional trends and spatial distribution of key sources, Non-CO_2 Greenhouse Gases (NCGG-4), A. van Amstel (coord.), pp. 325–330, Millpress, Rotterdam, Netherlands.

Olson, J. R., et al. (2001), Seasonal differences in the photochemistry of the PEM-Tropics A and B, *J. Geophys. Res.*, *106*, 32,749–32,766.

Olson, J. R., et al. (2004), Testing fast photochemical theory during TRACE-P based on measurements of OH, HO_2, and CH_2O, *J. Geophys. Res.*, *109*, D15S10, doi:10.1029/2003JD004278.

Olson, J. R., J. H. Crawford, G. Chen, W. H. Brune, I. C. Faloona, D. Tan, H. Harder, and M. Martinez (2006), A reevaluation of airborne HO_x observations from NASA field campaigns, *J. Geophys. Res.*, *111*, D10301, doi:10.1029/2005JD006617.

Oshima, N., et al. (2004), Asian chemical outflow to the Pacific in late spring observed during the PEACE-B aircraft mission, *J. Geophys. Res.*, *109*, D23S05, doi:10.1029/2004JD004976.

Park, R., D. J. Jacob, B. D. Field, R. M. Yantosca, and M. Chin (2004), Natural and transboundary pollution influences on sulfate-nitrate-anmonium aerosols in the United States: Implications for policy, *J. Geophys. Res.*, *109*, D15204, doi:10.1029/2003JD004473.

Parrish, D. D., Y. Kondo, O. R. Cooper, C. A. Brock, D. A. Jaffe, M. Trainer, T. Ogawa, G. Hübler, and F. C. Fehsenfeld (2004a), Intercontinental Transport and Chemical Transformation 2002 (ITCT 2K2) and Pacific Exploration of Asian Continental Emission (PEACE) experiments: An overview of the 2002 winter and spring intensives, *J. Geophys. Res.*, *109*, D23S01, doi:10.1029/2004JD004980.

Parrish, D. D., et al. (2004b), Changes in the photochemical environment of the temperate North Pacific troposphere in response to increased Asian emissions, *J. Geophys. Res.*, *109*, D23S18, doi:10.1029/2004JD004978.

Pierce, R. B., et al. (2003), Regional Air Quality Modeling System (RAQMS) predictions of the tropospheric ozone budget over east Asia, *J. Geophys. Res.*, *108*(D21), 8825, doi:10.1029/2002JD003176.

Richter, A., J. P. Burrows, H. Nüß, C. Granier, and U. Niemeier (2005), Increase in tropospheric nitrogen dioxide over China observed from space, *Nature*, *437*, 129–1323.

Streets, D. G., et al. (2003), An inventory of gaseous and primary aerosol emissions in Asia in the year 2000, *J. Geophys. Res.*, *108*(D21), 8809, doi:10.1029/2002JD003093.

Streets, D. G., Q. Zhang, L. Wang, K. He, J. Hao, Y. Wu, Y. Tang, and G. R. Carmichael (2006), Revisiting China's CO emissions after the Transport and Chemical Evolution over the Pacific (TRACE-P) mission: Synthesis of inventories, atmospheric modeling, and observations, *J. Geophys. Res.*, *111*, D14306, doi:10.1029/2006JD007118.

Takegawa, N., et al. (2004), Removal of NO_x and NO_y in Asian outflow plumes: Aircraft measurements over the western Pacific in January 2002, *J. Geophys. Res.*, *109*, D23S04, doi:10.1029/2004JD004866.

Tanimoto, H., Y. Sawa, H. Matsueda, I. Uno, T. Ohara, K. Yamaji, and S. Yonemura (2005), Significant latitudinal gradient in the surface ozone spring maximum over East Asia, *Geophys. Res. Lett.*, *32*, L21805, doi:10.1029/2005GL023514.

Thompson, A. M. (1992), The oxidizing capacity of the Earth's atmosphere: Probable past and future changes, *Science*, *256*, 1157–1165.

Thornton, J., and J. P. D. Abbatt (2005), Measurements of HO_2 uptake to aqueous aerosol: Mass accommodation coefficients and net reactive loss, *J. Geophys. Res.*, *110*, D08309, doi:10.1029/2004JD005402.

Thornton, J. A., et al. (2002), Ozone production rates as a function of NO_x abundances and HO_x production rates in the Nashville urban plume, *J. Geophys. Res.*, *107*(D12), 4146, doi:10.1029/2001JD000932.

Thornton, J. A., C. F. Braban, and J. P. D. Abbatt (2003), N_2O_5 hydrolysis on sub-micron organic aerosol: The effect of relative humidity, particle phase and particle size, *Phys. Chem. Chem. Phys.*, *5*, 4593–4603.

Tie, X., G. Brasseur, L. Emmons, L. Horowitz, and D. Kinnison (2001), Effects of aerosols on tropospheric oxidants: A global model study, *J. Geophys. Res.*, *106*, 22,931–22,964.

Wang, Y., J. A. Logan, and D. J. Jacob (1998), Global simulation of tropospheric O_3-NO_x-hydrocarbon chemistry: 2. Model evaluation and global ozone budget, *J. Geophys. Res.*, *103*, 10,727–10,755.

Wild, O., et al. (2004a), Chemical transport model ozone simulations for spring 2001 over the western Pacific: Regional ozone production and its global impacts, *J. Geophys. Res.*, *109*, D15S02, doi:10.1029/2003JD004041.

Wild, O., P. Pochanart, and H. Akimoto (2004b), Trans-Eurasian transport of ozone and its precursors, *J. Geophys. Res.*, *109*, D11302, doi:10.1029/2003JD004501.

Yienger, J. J., A. A. Klonecki, H. Levy II, W. J. Moxim, and G. R. Carmichael (1999), An evaluation of chemistry's role in the winter-spring ozone maximum found in the northern midlatitude free troposphere, *J. Geophys. Res.*, *104*, 3655–3667.

————————————

D. R. Blake and I. J. Simpson, Department of Chemistry, University of California, Irvine, Irvine, CA 92697-2025, USA. (drblake@uci.edu; isimpson@uci.edu)

G. Chen and M. Ko, Langley Research Center, National Aeronautics and Space Administration, Hampton, VA 23681, USA. (g.chen@larc.nasa.gov; malcolm.k.ko@larc.nasa.gov)

R. C. Hudman, Division of Engineering and Applied Sciences, Harvard University, 29 Oxford Street, Cambridge, MA 02138, USA. (hudman@fas.harvard.edu)

S. Kawakami, Earth Observation Research and Application Center, Japan Aerospace Exploration Agency, Tokyo, Japan.

K. Kita, Department of Environmental Science, Ibaraki University, Bunkyo 2-1-1, Mito, Ibaraki 310-8512, Japan. (kita@env.sci.ibaraki.ac.jp)

M. Koike, Earth and Planetary Science, Graduate School of Science, University of Tokyo, 7-3-1 Hongo, Bunkyo-ku, Tokyo 113-0033, Japan. (koike@eps.s.u-tokyo.ac.jp)

Y. Kondo, Y. Miyazaki, and N. Takegawa, Research Center for Advanced Science and Technology, University of Tokyo, 4-6-1 Komaba, Meguro-ku, Tokyo 153-8904, Japan. (y.kondo@atmos.rcast.u-tokyo.ac.jp; yuzom@atmos.rcast.u-tokyo.ac.jp; takegawa@atmos.rcast.u-tokyo.ac.jp)

K. Nakamura, Department of Resources and Environmental Engineering, School of Creative Science and Engineering, Faculty of Science and Engineering, Waseda University, Tokyo 169-8555, Japan. (kenji.nakamura@aoni.waseda.jp)

T. Shirai, Center for Global Environmental Research, National Institute for Environmental Studies, Tsukuba, Ibaraki 305-8506, Japan. (tshirai@nies.go.jp)